AD-A049 796 BRISTOL UNIV (ENGLAND) H H WILLS PHYSICS LAB F/G 11/4
THE PHYSICAL MECHANISMS RESPONSIBLE FOR THE WEATHERING OF EPOXY--ETC(U)
OCT 77 N R FARRAR, T W TURNER, K H ASHBEE DA-ERO-76-G-068

UNCLASSIFIED NL

1 OF 1
AD
A049 796

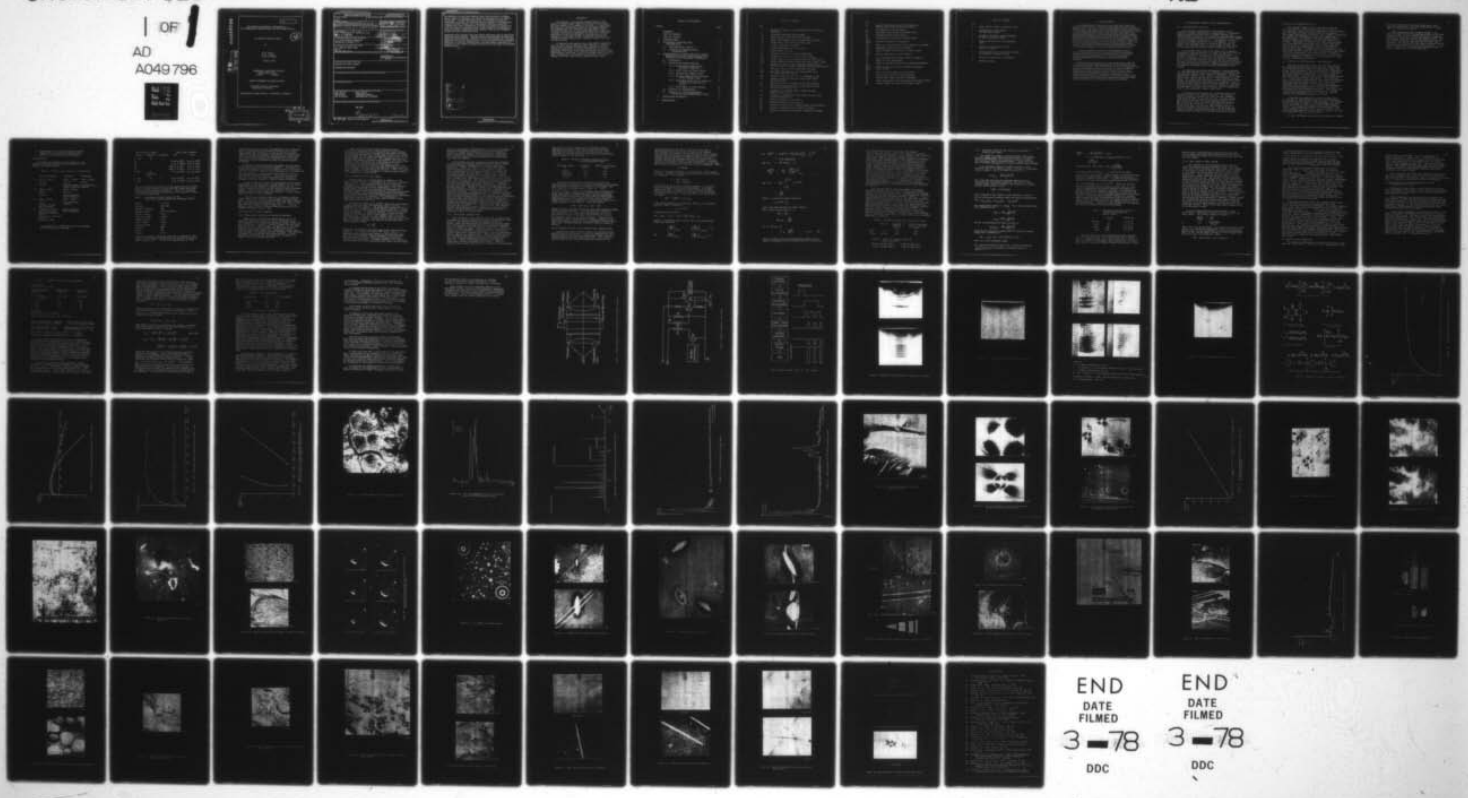

END
DATE
FILMED
3-78
DDC

END
DATE
FILMED
3-78
DDC

AD A049796

AD No.
DDC FILE COPY

AD

The Physical Mechanisms Responsible for the Weathering of Epoxy Resins and GFR Epoxy Resins

12

1st Annual Technical Report

by

N. R. Farrar
T. W. Turner
K. H. G. Ashbee

October 1977

EUROPEAN RESEARCH OFFICE
United States Army
London England

GRANT NUMBER DA-ERO-76-G-068

H. H. Wills Physics Laboratory
University of Bristol

Approved for Public Release; distribution unlimited

DDC
RECEIVED
FEB 10 1978
B

UNCLASSIFIED

SECURITY CLASSIFICATION OF THIS PAGE (When Data Entered)

REPORT DOCUMENTATION PAGE

READ INSTRUCTIONS BEFORE COMPLETING FORM

1. REPORT NUMBER (6)

2. GOVT ACCESSION NO.

3. RECIPIENT'S CATALOG NUMBER

4. TITLE (and Subtitle)
THE PHYSICAL MECHANISMS RESPONSIBLE FOR THE WEATHERING OF EPOXY RESINS AND GFR EPOXY RESINS.

5. TYPE OF REPORT & PERIOD COVERED
(9) ANNUAL REPORT. NO. 1,
SEP 76 — OCT 77,

6. PERFORMING ORG. REPORT NUMBER

7. AUTHOR(s)
(10) N. R. FARRAR, T. W. TURNER
[redacted] K. H. G. ASHBEE

8. CONTRACT OR GRANT NUMBER(s)
(15) DAERO-76-G-068

9. PERFORMING ORGANIZATION NAME AND ADDRESS
H. H. WILLS PHYSICS LABORATORY
UNIVERSITY OF BRISTOL, U.K.

10. PROGRAM ELEMENT, PROJECT, TASK AREA & WORK UNIT NUMBERS
(16) 6.11.02A-1T161102BH57-
(17) 00-598

11. CONTROLLING OFFICE NAME AND ADDRESS
(11) U.S. ARMY R&S GROUP (EUR)
BOX 65
FPO NEW YORK 09510

12. REPORT DATE
OCT[redacted] 77

13. NUMBER OF PAGES
(12) 78p.

14. MONITORING AGENCY NAME & ADDRESS (if different from Controlling Office)

15. SECURITY CLASS. (of this report)
UNCLASSIFIED

15a. DECLASSIFICATION/DOWNGRADING SCHEDULE

16. DISTRIBUTION STATEMENT (of this Report)
APPROVED FOR PUBLIC RELEASE

DISTRIBUTION UNLIMITED

17. DISTRIBUTION STATEMENT (of the abstract entered in Block 20, if different from Report)

18. SUPPLEMENTARY NOTES

19. KEY WORDS (Continue on reverse side if necessary and identify by block number)

EPOXY RESINS	WATER DAMAGE
GFR EPOXIES	ULTRASONIC IMAGING
NDT OF EPOXIES	DETERIORATION OF EPOXIES

20. ABSTRACT (Continue on reverse side if necessary and identify by block number)

SEE OVER

S/N 393113

DD FORM 1 JAN 73 1473 EDITION OF 1 NOV 65 IS OBSOLETE

UNCLASSIFIED

SECURITY CLASSIFICATION OF THIS PAGE (When Data Entered)

The technique of using high intensity light emitting diodes to produce optical images of ultrasonic wave trains has been applied to two aspects of the work. In experiments preliminary to fundamental studies of resin/glass interfaces, the technique has been refined to the stage where clearly resolvable fringes can be reproducibly observed in glass and in epoxy resin, and in experiments to assess the technique's potential as a NDT tool capable of detecting flaws in real composites, ultrasound has been successfully transmitted through composite slabs to give 'readable' fringes in a glass visualising block.

Accelerated water exposure tests and natural weathering tests on epoxy resin composites have continued. Chemical analysis has confirmed the impression gained from microstructural examination of fracture surfaces that, even when apparently fully cured, these materials contain unreacted resin and hardener, dissolution of which by diffused water is no doubt partly responsible for generation of the pockets of pressure believed to be the cause of disc-shaped internal cracks.

ACCESSION for
NTIS White Section ✓
DDC Buff Section ☐
UNANNOUNCED ☐
JUSTIFICATION
BY
DISTRIBUTION/AVAILABILITY CODES
Dist. AVAIL. and/or SPECIAL
A

SUMMARY

The technique of using high intensity light emitting diodes to produce optical images of ultrasonic wave trains has been applied to two aspects of the work. In experiments preliminary to fundamental studies of resin/glass interfaces, the technique has been refined to the stage where clearly resolvable fringes can be reproducibly observed in glass and in epoxy resin, and in experiments to assess the technique's potential as a NDT tool capable of detecting flaws in real composites, ultrasound has been successfully transmitted through composite slabs to give 'readable' fringes in a glass visualising block.

Accelerated water exposure tests and natural weathering tests on epoxy resin composites have continued. Chemical analysis has confirmed the impression gained from micro-structural examination of fracture surfaces that, even when apparently fully cured, these materials contain unreacted resin and hardener, dissolution of which by diffused water is no doubt partly responsible for generation of the pockets of pressure believed to be the cause of disc-shaped internal cracks.

TABLE OF CONTENTS

Section		Page
	SUMMARY	
	LIST OF FIGURES	
	LIST OF TABLES	
1.	INTRODUCTION	1
2.	ULTRASONIC PHOTOELASTIC EXPERIMENTS	2
	2.1 EXPERIMENTAL SET-UP	2
	2.2 RESULTS OF PHOTOELASTIC EXPERIMENTS	3
3.	MECHANISMS OF WATER DAMAGE IN EPOXY RESINS AND IN GFR EPOXY RESINS THAT CONTAIN WATER SOLUBLE INCLUSIONS	5
	3.1 MATERIALS	5
	3.2 RESULTS ON RESIN SAMPLES	7
	3.2.1 Measurements Made During Specimen Preparation	7
	3.2.2 Initial Effects of Water Uptake	8
	3.2.3 Internal Disc-shaped Cracks	9
	3.2.4 Original Model for the Formation of Disc-shaped cracks	10
	3.2.5 Alternative Model for the Conversion of Pockets of Pressure into Cracks	14
	3.2.6 Later Stages of Water Damage	16
	3.3 RESULTS ON COMPOSITES	17
	3.4 RESULTS OF WATER IMMERSION TESTS AND ENVIRONMENTAL TESTS	18
4.	CONTINUING RESEARCH	21
5.	REFERENCES	

LIST OF FIGURES

No.

1. Principal Components of the Photoelastic Visualisation Technique.
2. Ultrasonic transducer driver stage.
3. Block diagram of the TTL LED circuitry.
4. Single and multiple pulses in fused quartz (2 MHz)
5. 2 MHz pulses after passing through steel.
6. Fringes illuminated in quartz.
7. 2 MHz longitudinal and shear waves.
8. Ideal DGEBA structure.
9. Chemical structures of system components.
10. Weight loss with cure time for type A resin.
11a. Weight change against immersion time in 100°C water.
11b. Linear expansion against immersion time in 100°C water.
12. Variation of time to reach maximum weight (x) and time to return to original weight (•) with specimen thickness.
13. Fracture surface to show spherulitic structure.
14a. Gas chromatograph total ion current (TIC) trace for 100°C immersion water.
14b. Computed mass spectrum of one component of TIC.
15. Flame ionisation for (a) pure water and (b) 100°C immersion water.
16. Scanning electron micrograph of internal cracking.
17. Stress birefringence around internal cracks viewed (a) face-on and (b) edge-on.
18. Comparison of internal cracks viewed with and without crossed polars.
19. Variation of birefringence with strain for epoxy resin at room temperature.
20. Internal cracking in resin type A.
21. Internal cracking in resin type C.
22. Cracking of resin type C viewed through crossed polars.
23. Internal cracking around an impurity inclusion.
24. Optical and electron micrograph of spherical cracking.

No.	
25.	Sequence showing growth of air bubble in an internal crack after removal from water.
26.	Air bubbles in internal cracks.
27.	Condensed water around an internal crack.
28.	Condensed water around cracks.
29.	'Wormholes' growing from internal cracks.
30a. 30b.	Internal structures of 'wormholes'
30c.	Model for craze production (after Beahan et al. (1972)).
31a.	Impurities visible in face-on cracks.
31b.	Crack initiation centre seen in cut away crack.
32. 33.	SEM of impurities on crack surfaces.
34.	X-ray spectrum from particle shown in figure 32.
35.	Stages of resin degradation.
36.	SEMs of internal structure after extreme degradation.
37. 38. 39.	SEMs of internal structures formed by extreme water etching.
40.	SEMs of earlier stages in water etching.
41.	Glass fibres before and after debonding.
42.	Carbon fibres before and after debonding.
43.	Stress birefringence and around glass and carbon fibres.
44.	Surface bubbles on silane covered glass fibres.

LIST OF TABLES

No.

1. Resin systems used in the present work

2. Composition of CIBA-GEIGY MY 750 epoxy resins

3. Results of inorganic chemical analysis of 100° C immersion water.

4. Osmotic pressures for two potassium salts.

5. Results of mechanical tests for epoxy resin (A2).

6. Pressure and energy required to stabilise the formation of 'penny' cracks.

7. Results of curing stress calculations.

8. Surface energies.

1. INTRODUCTION

An essential feature of the weathering of glass fibre reinforced resins is the destruction of adhesion between glass and solid resin by diffused water. The nature of accommodation by the resin of obstruction to resin dimensional changes during water uptake is believed to be central to the destruction process, that is, that the build-up of elastic and possibly plastic strain in resin immediately adjacent to fibres and the enhancement of chemical reactions by such strain is believed to play a prominent role in mechanisms responsible for loss of adhesion. The build-up of local strains is unlikely to alter the densities of interfacial bonds and the failure of high resolution techniques (ESCA, SIMS, etc.) to detect significant differences in bond densities between failures obtained after exposure to different aqueous environments is taken as circumstantial evidence for the line of approach presented here.

Sensitive methods are needed for investigating the states of stress and strain at glass/resin interfaces and for monitoring changes in these states of stress and strain during water uptake. A supplementary research grant (77-G-071) has been made available to develop a visualisation of ultrasound method for doing this.

Although stress enhanced attack of interfacial bonds is believed to be at the nub of the weathering problem, in real composites, that is in dirty composites, there are additional problems arising from the presence of impurity inclusions, interaction of which with diffused water leads to resin fractures and to interfacial failure. The identification in this laboratory (Ashbee, Frank and Wyatt 1967;[1] Ashbee and Wyatt 1969)[2] of mechanisms responsible for these problems in polyester resin composites was the basis of the original research proposal (76-G-068) and the mechanisms identified in that early work have now been identified in epoxy resin systems.

2. ULTRASONIC PHOTOELASTIC EXPERIMENTS

2.1 EXPERIMENTAL SET-UP

The principles of photoelastic stress analysis can be utilised to visualise high frequency stress waves in a transparent medium as shown by Wyatt (1972, 1975)[3,4] and Andrews and Wallis (1977).[5] Stroboscopic illumination is controlled electronically to create standing waves of the dynamic birefringence field, which are viewed through crossed polars. The diagram in figure 1 shows the principal components of the arrangement. An LED provides the light with lenses to collimate and converge the beam. This visualising block of glass, quartz or epoxy resin, is placed between the crossed polarizer and analyser plates.

An ultrasonic wave packet is generated in the transducer by applying a high voltage pulse to a wafer of 'Vernitron' PZT 5A piezoelectric material using an A. E. I. XT 2104 801 pulse modulator thyrister. The repetition rate of the pulse is 3 kHz for visual observation, but this may be reduced for photographic work. This reduced frequency gives time for the reflections of the sound waves from the previous pulse to die away and eliminate a background stress wave pattern. Higher frequencies are used for visual work because of the increased illumination of the fringes.

To obtain the stroboscopic illumination, a Hewlett-Packard type 5082-4558 high intensity LED is flashed in synchronism with the resonant frequency of the ultrasonic transducer. Single or multiple light flashes can be used up to frequencies of ~ 10 MHz with a pulse width of typically 50 ns. With accurately crossed polars, both compressive and tensile stresses give bright fringes, and the wavelength of the sound appears to be halved. With a retardation plate included however, placed between the visualising medium and the analyser, compensation is possible to allow for the retardation of compression and tension, and an adjustment is made to give extinction at either stress level.

A simplified circuit diagram for the driver stage to the ultrasonic transducer is shown in figure 2. The oscillator which determines a repetition rate from 500 Hz to 3000 Hz sends positive pulses to the base for TR1. Current supplied from the 20 v line can now flow through the primary P1 of the transformer, and the secondary S2 (1:40 ratio) develops 800 v across the transducer. A negative pulse from S1 (P1/S1 turns ratio 1:1) switches TR2, allowing current to flow to the trigger of the thyrister TH1. The thyrister now conducts rapidly, removing the charge across the transducer electrodes and resulting in an ultrasonic ring at the resonant

frequency of the piezoelectric disc.

The thyrister trigger pulse is also used to start the TTL LED circuitry, shown in block diagram in figure 3. A potentiometer controls the delay monostable to set the distance the sound wave will have travelled before it is visualised. This triggers the enabling monostable, also variable, to determine the length of the LED pulse train to give a single pulse or multiple flashes. An oscillator chops the enabling pulse to match the ultrasonic frequency and is variable from 0.5 to 10 MHz. Each pulse is shaped by the flash time monostable whose variable timing components allow a pulse width range from 30 to 100 ns. Eight NAND gates in parallel provide the necessary current amplification to drive the common emitter output stage. A third line of 35 v provides the LED with power, and by running the LED at temperatures approaching -195°C the illumination is increased threefold. Although of marginal value for photographic work, better illumination has made the technique a much more viable proposition for visual scrutiny of diffraction phenomena.

2.2 RESULTS OF PHOTOELASTIC EXPERIMENTS

Since the first periodic report, the electronics driving the ultrasonic transducer have been improved. With better TTL controlling a near square wave train to the LED, clear fringes can be observed in the visualising block. Although the results presented here are with a quartz block, fringes have also been observed in Steuben glass, in soda glass and in 1009 epoxy resin. Figure 4 shows single and multiple flashes from a 2 MHz pulse in the fused quartz. The longitudinal waves can be seen travelling directly down from the transducer, which is visible top centre, with the shear waves of shorter wavelength clearly resolved at 45° on each side of the longitudinal wave direction. The single flash photograph also shows the diamond-shaped pattern resulting from multiple reflections from the preceding sound pulse. This pattern can be removed by slowing down the repetition rate. Another multiple flash photograph is shown in figure 5. Here the sound has first passed through 13 mm of steel.

A specimen was prepared by cutting a section from a 10" diameter ½" wall thickness GRP tube and sited between the transducer and the quartz visualising block. The resulting fringes are shown in figure 6. Two photographs are taken with 3 pulses and two with pulses from the LED flashing at 2 MHz. Two images are included to demonstrate the effect of the composite compared with no specimen present. By taking the photograph near to the edge of the quartz, the mode converted shear wave can be seen clearly.

To date, information arising from the presence of defects

has been established using simpler single phase solids, especially with metals: this work is the basis of a paper which will shortly be available.

While investigating the transducer design, it was found that soldering the PZT piezoelectric disc to the brass transducer body, is more effective and leads to a greater efficiency as reported by Gutfeld and Melcher (1977).[6] This constraining of the PZT disc has the added advantage that the mode of oscillations which produce the shear wave is increased. Longitudinal and shear waves generated from the same transducer have already been seen in figure 4 , and figure 7 shows both waves again after passing through the 8.35 mm thick wall of the composite tube.

3. MECHANISMS OF WATER DAMAGE IN EPOXY RESINS AND IN GFR EPOXY RESINS THAT CONTAIN WATER SOLUBLE INCLUSIONS

3.1 MATERIALS

The epoxy resin systems used to search for water damage of the kind previously found in polyester resin systems are listed in table 1.

Table 1. Resin systems used in the present work

	Resin identification	Hardener	Accelerator
A	CIBA - GEIGY MY 750 DGEBA	CIBA - GEIGY HY 917 Methyltetrahydro-phthalic anhydride	CIBA - GEIGY DY 062 triamylammonium phenate
B	CIBA - GEIGY MY 756 DGEBA	CIBA - GEIGY HT 973 Boron trifluoride Mono-ethylamine	
C	CIBA - GEIGY MY 753 DGEBA + 16.66% dibutyl phthalate	CIBA - BEIGY Polyoxypropylene triamine	
D	67% DOW DEN 538 Polyglycidyl ether of phenol formaldehyde novolac +33% SHELL EPON 828 DGEBA (mix code 1009)	Boron trifluoride Mono-ethylamine	

The proportions by weight and resin cure schedules are continued on the next page.

Proportions by weight			Resin cure schedules	
Resins:	hardener:	accelerator	Gel	Cure
A 100	85	2		
A1			16 hr at 60°C	4 hr at 150°C
A2			2 hr at 100°C	4 hr at 150°C
A3			2000 hr at 20°C	4 hr at 150°C
A4			2000 hr at 20°C	4 hr at 90°C
B 100	27 (in acetone :75)	-	7 hr at 100°C	2 hr at 200°C
C 100	33	-	24 hr at 20°C	6 hr at 60°C
D 100	3	-	$\frac{3}{4}$ hr at 165°C	4 hr at 177°C

The MY 750 resin used for most of the experiments is a medium viscosity DGEBA resin of average molecular weight 330 and the chemical formula is shown in figure 8 for n = 0. Ratcliffe and Weatherall (1976)[7] have analysed this resin and table 2 shows a summary of their data.

Table 2. Composition of CIBA-GEIGY MY 750 epoxy resins (after Ratcliffe and Weatherall (1967))[7]

Density	1.17 g/cc
Viscosity	120 poise
Epoxide equivalent	190
Hydroxyl content	0.05 mole/100 g
Chlorine content	0.5%
Molecular weight	324-337
Volatile content	0.4%
Water content	0.03%
Refracive index	1.571
Monomer	80%
Dimer	9%
Trimer	2.5%

In order to produce a thermoset resin that is resistant to water attack MY·917 hardener was selected, the structure of which is shown in figure 9a. Since this compound does not react

directly with the epoxy group, ring opening by active hydrogens has to be provided by an accelerator (DY 062 in this case). The hardener then behaves as an acid and the two principal chemical reactions are addition esterification and etherification. Many factors determine the rate and path of the reaction and it is only by way of empirical methods that the correct mix proportions may be determined in order to produce required properties.

One resin system known to be susceptible to water attack is MY 750 resin used with HT 973 hardener. The latter is a Lewis acid complex, the formula of which is shown in figure 9b The cure reaction is rapid at room temperature for BF_3 alone and the monoethylamine is added to block the reactivity, up to its dissociation temperature ($\sim 90^{o}C$). Both these systems are hot-cure systems in that high temperatures are required to initiate the reaction and also to remove volatile by-products.

A low temperature system was also chosen for the present investigations. The resin was a normal DGEBA resin modified with 16.66% dibutyl phthalate, (formula shown in fig. 9c which decreases the viscosity of the resin and thereby facilitates mixing. The MY 753 is cured with a triamine, see fig. 9d which by contrast with the previous systems, is a basic curing agent and reacts by amine addition.

A fourth resin system selected for investigation used the Lewis acid complex hardener, with an epoxy resin mix coded 1009. This is a mix of a normal DGEBA resin (Shell Chemical Co. EPON 828) and Dow Chemical Co. DEN 438, novolac resin (the formula of which is shown in figure 9e , It is a hot-cure system which is currently being characterised at the AMMRC Watertown, Mass., USA.

3.2 RESULTS ON RESIN SAMPLES

3.2.1 Measurements made during specimen preparation

Although epoxy resins do not shrink during cure to the extent that polyesters do there is still an observable effect and measurements of weight and dimensional changes during cure were carried out. Figure 10 shows the weight loss with cure time for the type A resin system. In general, 4 hrs at $150^{o}C$ produces a 0.4% weight loss while the same time at $90^{o}C$ results in only 0.04% weight loss. Dimensional changes after 4 hrs at $150^{o}C$ were around 1% linear shrinkage. Such decreases in weight and size probably result from emission of volatile impurities, released as the cure progresses, resulting in a tighter, denser cross-linked structure.

Many specimens were stored for some time before testing and, during this time, there occurred a small increase in weight presumably due to absorption of atmospheric moisture. The quantities absorbed were of the order of 0.4% in 20 months but the weight loss on curing remained only about 0.5%, i.e. an overall weight loss of only 0.1%. This implies that water has attacked the chemical structure of the network and become bound. However, this is plausible only if the energy of the bond is greater than the thermal energy provided during curing. Alternatively the period of time at room temperature may have seen a gradual cure such that cross-linking is complete and only absorbed water is emitted during the full cure. This is the more likely explanation, but the possibility of bound adsorbed moisture is reconsidered in section 3.2.6.

3.2.2. Initial effects of water uptake

Boiling water has a marked effect on samples of resin types A1, A2, B and C. Such exposure is, of course, extremely severe and the results presented below may not accurately extrapolate to the performance of the resin systems exposed to aqueous environments at lower temperatures. The use of boiling water accelerates the processes of degradation and facilitates detection and observation during a reasonable time-scale of a few months. From measurements on epoxy and polyester resins Stone (1968)[8] found overall activation energies for degradation machanisms of 15 to 33 kcal/mole. An average value of 24 kcal/mole implies that the reaction rate at 100°C is about 7000 times faster than at 20°C.

Immersion in boiling water initially causes the resin samples to gain weight and swell, see figures 11 a and b. However equilibrium is not reached. The weight and swelling give way to weight loss and shrinkage presumably because material is leached out of the matrix. The specimen thickness affects the time-scale involved and figure 12 shows how the time to reach maximum weight and the time to return to the original weight vary with the sample size. The rate of water diffusion may be estimated from such data as follows. Assuming that a whole specimen 1 mm thick is uniformly saturated with water in 150 hrs (the time to reach maximum weight)

$$D \sim \frac{x^2}{t}$$

where D is the diffusion coefficient and x is the distance diffused in time t. D is found to be about 10^{-8} cm^2/s and is in agreement with previous measurements on thermosetting resins (Lee and Neville (1967)).[9] Chemical analysis of the immersion water has shown that both organic and inorganic material is extracted from the matrix. Inorganic impurities are believed to be introduced during resin manufacture and curing, and the organic

material is attributed to unreacted parts of the resin formulation. Although stoichiometric proportions of resin and hardener are mixed it is unlikely that the reaction proceeds to completion. Steric hindrance by regions of the network which harden first prevents the remaining unreacted molecules from approaching each other for reaction.

Much evidence has been reported on a granular structure in epoxy resins (for example Cuthrell (1967)[10] and Schoon (1970)[11] and the observations presented below strongly support this hypothesis. Figure 13 shows a room temperature tensile fracture surface of a fully cured sample of type A resin. It shows a 'spherulitic' type structure as might be expected if the cure reaction began at many different centres from which it proceeded radially until the 'grains' touched. Any unreacted resin or hardener is expected to be deposited between the grains and in diffused water such deposits are likely to be more soluble than fully cured material. One possible consequence of dissolution of unreacted constituents is the immobilisation of diffused water and this is further discussed in this section later. Analysis of the immersion water has identified chemical groups from the hardener molecule. Figure 14 shows a gas chromatograph total ion current (TIC) trace and the computed mass spectrum of one separated component. The fig. 14b peaks are derivatives and isomers of a di-acid and are produced by the interaction of water with the acid anhydride hardener of resin system A. Figure 15 shows the flame ionisation traces of the separated volatile components from pure water and immersion water and these indicate the presence of the same acid groups which seem to comprise 2% by weight of the immersion water. Inorganic analyses have also identified ions of various salts in the immersion water and some data are shown in table 3. Analysis of the resin itself by Ratcliffe and Weatherall (1967)[7] revealed the presence of 0.5% chlorine content of which 0.3% is hydrolisable and therefore amenable to attack by diffused water.

3.2.3 Internal disc shaped cracks

The dissolution of water solubles also leads to further resin degradation in the form of internal cracking, an example of which is seen in the scanning electron micrograph of figure 16 Similar cracks have been previously observed in polyester resins after much shorter immersion times and a qualitative hypothesis based on osmosis has been proposed by Ashbee et al. (1967)[1] in order to account for them. A semi-quantitative treatment of their mechanism is developed in section 3.2.4. In the commercial epoxies studied here, external cracks begin to develop after about 150 hrs immersion in boiling water. When first formed they are best detected by observation of the stress birefringence arising from their associated deformation of the surrounding resin. Figure 17 shows cracks observed face-on and edge-on respectively and their associated stress fields. Figure 18 shows two more cracks seen directly and through crossed polaroids.

The cracks are disc shaped and are randomly oriented throughout the sample. They grow in size from an initial diameter of about 2 μm after about 150 hrs to over 1 mm after 400 hrs at which time they often distort and fracture the external surface of the specimen.

Table 3. Results of inorganic chemical analysis of 100°C immersion water

Parts per million of	Distilled water	2000 hrs immersion water
Sodium	2.0	4.0
Potassium	4.0	19.0
Calcium	2.0	3.0

The signs and magnitudes of the stresses around disc cracks have been determined from optical retardation measurements. The stress-optic coefficient of resin type A, for example, has been found from the graph shown in figure 19 to be -4×10^{-12} m^2/N. This is much smaller and of opposite sign to the value usually quoted in the literature (see for example, Kuske and Robertson (1974)).[12] However, repeated experiments on many samples confirm that the coefficient is indeed negative. Measurements in the resin adjacent to disc cracks reveal a negative retardation corresponding to a compressive stress in the radial direction of about 200 nm. Using the formula

$$C\,(\sigma_1 - \sigma_2) = (n_1 - n_2) = \frac{R}{d}$$

implies that the difference between the axial and tangential principal stresses is about 500 bars. C is the stress-optic coefficient, R is retardation, d $\sim$ 1mm is specimen thicknes, σ_1, σ_2 are the principal stresses in the plane considered and n_1, n_2 are the refractive indices in the same directions. Different resin formulations produce crack patterns of different appearance and while those shown in figure 20 are representative of resin type A, resin type C develops patterns of the form shown in figures 21 and 22.

3.2.4 Original model for the formation of disc shaped cracks

Internal disc shaped cracks in resins are attributed to the following osmotic mechanism. It has been established (loc. sit.) that the epoxy resins used here contain water soluble inclusions, including organic salts and organic molecules. When diffused water reaches such an inclusion dissolution commences, the

chemical potential of the solution will be less than that of the immersion water and by way of osmosis, the gradient will stimulate the creation of a pressure located at the inclusion. Although strong electrolytic solutions and high polymer solutions deviate from ideal solutions the following analysis for ideal solutions will provide estimates of the order of magnitude of the osmotic pressure generated by the above mechanism. Chemical potential is equivalent to partial molar free energy and represents the increase in energy due to increase in mass of material. Hence

$$\mu = \partial E / \partial n$$

where μ is chemical potential, E is energy and n is the number of moles. A chemical potential gradient produces mass movement to equilibrium. For a solution

$$\begin{aligned} \mu &= \mu^0 + RT \ln a \\ &= \mu^0 + RT \ln xf \end{aligned}$$

where μ^0 is the pure solvent chemical potential, a is activity, x is concentration and f is activity coefficient. In an ideal solution f is unity. Addition of solute to solvent produces a decrease in vapour pressure over the solution and is reflected by decreases in a and μ. Using subscripts 1 for solvent and 2 for solute

$$\mu_1^{vap} = (\mu_1^0)^{vap} + RT \ln p_1$$

if the vapour behaves as an ideal gas, where p_1 is its partial pressure, which is defined by

$$p_1 = P\, x_1^{vap}$$

P being the total pressure.

Now $d\mu_1 = S_1 dT + V_1 dP + (\partial \mu_1 / \partial x_2)\, dx_2$

where S_1, the partial molar entropy and V_1 the partial molar volume are defined by

$$\left(\frac{\partial \mu}{\partial T}\right)_{P, x_2} = -\left(\frac{\partial S}{\partial n_1}\right)_{T, P, n_2} = -S_1$$

and

$$\left(\frac{\partial \mu}{\partial P}\right)_{T, x_2} = \left(\frac{\partial V}{\partial n_1}\right)_{T, P, n_2} = V_1$$

So $d\mu_1^{soln} = V_1 dP^{soln} + (\partial\mu_1/\partial x_2)^{soln}_{T,P} \; dx_2^{soln}$

$= 0$ for equilibrium

But $d\mu_1 = RT \, d \ln a_1$ so

$$\frac{dP^{soln}}{dx_2} = - \frac{RT}{V_1} \left(\frac{\partial \ln a_1}{\partial x_2}\right)_{T,P}$$

and $$\ln a_1 = \frac{1}{RT} \int_{p_1^0}^{p^{soln}} V_1 \, dP^{soln}$$

$$= - \frac{\pi V_1}{RT}$$

where π is osmotic pressure defined as

$$\pi = P^{soln} - p_1^0$$

and V_1 has been assumed to remain constant.

For a dilute solution when $f_1 = 1$

$$\ln a_1 = \ln x_1$$

$$\ln x_1 \simeq - \frac{\pi V_1}{RT}$$

or, as $\ln x_1 \simeq x_2$

$$\pi \simeq \frac{x_2 RT}{V_1} \qquad \text{———} \qquad 3.1$$

This is similar to the Van't Hoff equation usually used in osmosis calculations but its derivation does not assume that

the solution behaves like an ideal gas. For further consideration see Rossini (1950).[13] The equation is generally valid for solution concentrations up to 2 molar but for electrolytic solutions dissociation into ions requires a factor of 2 to be introduced. Other complications such as hydration and solvation also render this treatment inexact. The matrix must behave as a semi-permeable membrane and for permeation of large organic molecules this is likely to be the case although for small inorganic molecules and ions there may be grounds for doubt. However tests using solutions of inorganic salts as immersion liquids and resins doped with inorganic salts strongly suggest an osmotic process. When a salt solution is used as the immersion fluid there is a marked reduction in the extent of cracking and this is attributed to a smaller difference in chemical potential between the internal and surrounding liquid. Also when inorganic impurities are added to the resin there is a corresponding increase in the extent of cracking. Thus potassium chloride crystals introduced into specimens during mixing become clearly visible sites for crack generation, see figure 23.

Using formula 3.1 for saturated solutions of inorganic impurities osmotic pressures have been calculated and given in table 4. for two potassium salts. Tensile tests on samples of resin type A2 were carried out at room temperature and 100°C and yield the fracture strengths presented in table 5. It is evident that the pressures of table 4. are well above the tensile strength of the resin at 100°C and are therefore more than sufficient to cause failure. However, the pressure is hydrostatic and not uniaxially tensile across a plane so, unless there are large built-in compressive stresses it is not immediately obvious why disc shaped cracks form in preference to bubbles. In polyester resins a suitable biaxial compression arises as a consequence of the shrinkage which overtakes the initial resin swelling (Ashbee et al. 1967)).[1] However, large scale shrinkage does not accompany water uptake by epoxy resins so an alternative explanation is required.

Table 4. Osmotic pressures for two potassium salts

	mol. wt.	solubility at 100°C in g/litre	osmotic pressure of sat. soln. at 100°C in bars
KCl	74.56	567	480
KNO_3	101.11	2470	850

Table 5. Results of mechanical tests for epoxy resin (A2)

Tensile strength (20°C)	11,500 psi (800 bars)
Tensile strength (100°C)	4,000 psi (280 bars)

3.2.5 Alternative model for the conversion of pockets of pressure into cracks

The equilibrium shape of a pressure filled cavity is a flat penny-shape rather than spherical (Ashbee et al. 1973)).[14] Frank's (1973)[15] estimate of the pressure needed to stabilise the equilibrium shape is presented below. A correction by one of us (NRF) and approved by Frank (1977)[16] has been included.

In an isotropic medium of Young's modulus E, and Poisson's ratio ν, the elastic increase in volume of a spherical cavity of radius a, due to an internal pressure p, is

$$\Delta V_{e\ell} = \frac{2\pi(1+\nu)a^3 p}{E}$$

For a thin flat cavity the corresponding quantity may be calculated from the Griffith energy* U_G, (the elastic energy released when a crack is formed in the presence of a uniform uniaxial normal stress, σ,) and

$$U_G(\sigma) = \tfrac{1}{2}\sigma\,\Delta V_{e\ell}(\sigma)$$

where $\Delta V_{e\ell}(\sigma)$ is the volume of crack opening for stress σ. But internal pressure produces equal and opposite displacements. Thus $\Delta V_{e\ell}(p)/p = \Delta V_{e\ell}(\sigma)/\sigma = 2U_G(\sigma)/\sigma^2$

and elastic stored energy is $\frac{1}{2}p\Delta_{e\ell}$. For a penny shaped crack Sack (1946)[17] found that

$$U_G(\sigma) = \frac{8(1-\nu^2)a^3\sigma^2}{3E}$$

$$\Delta V_{e\ell} = \frac{16(1-\nu^2)a^3 p}{3E}$$

and the corresponding free energy decrease is

$$\tfrac{1}{2}p\Delta V_{e\ell} = \frac{8(1-\nu^2)a^3 p^2}{3E}$$

Including the surface free energy $2\pi a^2\gamma$ the total free energy change due to formation is

$$\Delta G = -pV_0 - 8(1-\nu^2)a^3p^2/3E + 2\pi a^2\gamma$$

where V_0 is the unstrained volume

*U_G equals the work done if the crack is closed up by applying internal tractions to its surfaces, rising from zero to σ. Here $p = \sigma$.

$$\frac{d(\Delta G)}{da} = -\frac{8(1-\nu^2)a^2p^2}{E} + 4\pi a\gamma$$

$$= 0, \text{ corresponding to maximum G when } a = a^* = \frac{\pi E\gamma}{2(1-\nu^2)p^2}$$

for which value $\Delta G = \Delta G^* = -pV_0 + \frac{\pi^3\gamma^3E^2}{6(1-\nu^2)^2p^4}$

For epoxy resin at 100°C, $E = 3.5 \times 10^8$ Nm^{-2} and taking $\nu = 0.34$ and $\gamma = 40$ mJm^{-2}, table 5. shows the internal pressure required to nucleate various sizes of cracks and the energy required to stabilise such cracks. At 100°C the thermal energy available is kT and assuming that a maximum barrier of 30 kT can be passed ΔG_{max} is 1.5×10^{-19} J. Hence the pressure required to stabilise the flat cracks is of the order of 1 kbar. This is comparable to the osmotic pressures calculated and strongly supports the mechanism proposed. It is possible that the value of γ may be changed by absorption of impurities and that the estimates of π are conservative especially for electrolytic solutions. Also, the above calculation pertains to a Hookean elastic matrix and after long immersion times the plasticising effect of water absorption will tend to invalidate such a treatment. Indeed, after very long exposures, the damage takes the form of spheroidal defects. Figure 24 shows examples of such damage as seen in the optical and electron microscope.

Table 6. Pressure and energy required to stabilise the formation of 'penny' cracks

a	P (bars)	ΔG(Joules)
100 μm	5	8×10^{-10}
1 μm	50	8×10^{-14}
10 nm	500	8×10^{-18}
1 nm	1600	8×10^{-20}

That the cracks are water filled when formed is deduced from the observation that, after removal from the immersion water, air bubbles can be seen to grow within them. Figure 25 shows a sequence of photographs which demonstrates this effect Also figure 26 shows air bubbles included within face-on cracks.

Measurements of the dark area around the inclusions and critical angle calculations enable the refractive index of the material within the cracks to be deduced and confirm that they are water filled.

3.2.6. Later stages of water damage

Water continues to be absorbed and reacts with the matrix by attacking the most hydrophilic bonds in the main resin chains such as hydroxyl and ether bonds. After periods of immersion in excess of 500 hrs apparently clear samples become opaque on removal from water and cooling to room temperature. This is attributed to condensation of water droplets into clusters which have displaced and now occupy weak sites in the matrix. The granular structure previously mentioned would give rise to gaps in the overall network once the low molecular weight material has been removed. Heating to 100°C in air removes this water but placing the specimen under high vacuum removes very little. Hence it appears that the molecules are bonded to the resin network and require thermal energy for release. The condensed droplets may be seen in figures 27 and 28 and it is noticeable that they do not form in the resin adjacent to internal cracks. Such regions are highly stressed and it appears that when one of the principal stresses is compressive the separation of the network to accommodate the water molecules is inhibited. Sneddon (1945)[18] has calculated the stresses around a penny-shaped crack and his results show that if the crack is inflated by an internal pressure, the surrounding stresses are such that there is no hydrostatic tension. Such a stress field would evidently assist the condensation of water.

It may be shown that the energy released by water condensation is sufficient to create fresh surfaces within the resin matrix. The Clausius Clapeyron equation is

$$\frac{d(\ell np)}{d(1/t)} = -\frac{\Delta H}{R}$$

so

$$\Delta H = -\frac{R[\Delta(\ell np)]}{\Delta(1/t)}$$

where ΔH is the energy change, p is the partial pressure of the vapour, T is the absolute temperature and R is the universal gas constant. During condensation the temperature drops from 100°C to 20°C and the vapour pressure of water changes from 760.00 mm Hg to 17.54 mm Hg. Hence

$$\Delta H = -897 \text{ J/mole} = 0.2 \text{ kcal/mole.}$$

A typical measured value for the quantity of absorbed water during condensation is 0.01 gms about 0.2 cals or 1 J. The surface energy of an epoxy resin is about 0.05 mJ/cm^2 so the energy release is sufficient to create 20 cm^2 of surface (neglecting the work done in storing elastic energy and also the energy of plastic deformation.) It is therefore plausible that the water clusters into groups within the resin network.

Also, after long periods of immersion, long tubular structures appear to grow from some cracks as shown in figure 29. The internal structure of these 'wormholes' (figure 30a and b) suggests that they may be crazes formed perpendicular to the principal tensile stress around the crack, somewhat similar to figure 30c taken from Beahan et al. (1972).[19] Alternatively, they may be formed by autocatalytic growth into the resin stimulated by impurity particles within the original crack. Possible impurities can be seen in the crack shown in figure 31a and the cut away crack in figure 31b Scanning electron microscope studies of the crack surfaces also show deposits of impurities as in figures 32 and 33. Electron probe X-ray microanalysis of these indicates the presence of several impurities including calcium and chlorine (which is known to be a by-product of manufacture). Figure 34 shows an element scan of the particle shown on figure 32 (the aluminium peak is from the microscope stub and the iron and copper are from the microscope.

Degradation continues and the resin backbone chain begins to lose its side-group after very long immersion times. Linear shrinkage reaches 8% and eventually, the sample transforms into a black sticky mass which becomes a brittle solid at room temperature. Figure 35 shows some of the stages of degradation and figure 36 shows the internal structure of the final state of degradation characterised by formation of a cell-structure. Severe degradation in other tests takes on a different form as the structures in figures 37, 38 and 39 show. This 'rosette' appearance could be a result of etching into the resin by the water. Electron probe X-ray microanalysis does not indicate the presence of any heavier elements ($Z > 12$) in the protuberances. This supports the hypothesis that the resin cures into granules, the 'spherulite' features in figures 37, 38 and 39 being the more highly cross-linked resin that remains after leaching out intermediate and low molecular weight materials. The size range of 1-5 μm for these features is within that of Lock (1972)[20] who produced similar effects by solvent etching. Figure 40 shows the earlier stages of this etching process in the present experiments.

3.3 RESULTS ON COMPOSITES

The composites examined here contained short fibres, some glass and other carbons. Fibres were cut to approximately 2 mm

lengths using a razor blade. They were degreased in acetone and dried in a warm oven. Glass fibres to be silane coated were mixed into a solution of 0.6 ml silane and 25 ml ethyl alcohol and 25 ml distilled water, for 5 mins. They were then dried in a warm oven. This procedure was used by Wyatt (1968)[21] to give the glass about a 0.5% by weight coating. The fibres were thoroughly mixed into the resin composition which was subsequently degassed under partial vacuum for $\frac{1}{2}$ hr before casting.

Hence 'standard' specimens were produced in three forms namely (1) containing short 10 μm diameter 'E' glass fibres, (2) containing short 9 μm diameter carbon fibres and (3) containing short 'E' glass fibres coated with a silane coupling agent.

3.4 RESULTS OF WATER IMMERSION TESTS AND ENVIRONMENTAL TESTS

Specimens of resin system A were immersed in boiling water and examined from time to time in the optical microscope. Here observations of the changes at resin/fibre interfaces are presented and discussed.

Before immersion, the specimens were examined; the fibre positions recorded and the birefringence in and around the fibres was measured. The full wavelength red plate was used to compare the signs of the stresses with those calculated and presented in table 7. The calculation was based on a theory by Poritsky, (1934)[22] modified by Wyatt (1968)[21] and gave good qualitative agreement with observations.

In most cases, debonding may be detected in either of two ways. One involves examination of the interface by eye in an attempt to detect a gap. The other relies on the measurement of stress in the fibre in order to determine when the interface ceases to transfer load. Figure 41a shows the appearance of glass fibres in the transmission optical microscope before water uptake. The refractive indices of the two materials are very close and the fibres are almost undetectable. Figure 41b shows a fibre after debonding when the interfacial gap has caused light scattering and the appearance of a dark band at the interface. For carbon fibres the appearance of debonding differs, as shown in figure 42 Figure 42a shows the bonded fibres and figure 42b a debonded fibre end.

Table 7.. Results of curing stress calculations

In the resin:
Axial stress = 9.5 psi

Radial coordinate (inches)	Radial stress (psi)	Hoop stress (psi)
4×10^{-4} (fibre surface)	-1.4×10^{5}	1.4×10^{5}
10^{-2}	-200	288
2×10^{-2}	- 42	70
3×10^{-2}	- 11	39
4×10^{-2}	0	28

In the fibre:
Axial stress = -9.5×10^{4} psi

Radial and hoop stresses = -1.4×10^{5} psi

Resin modulus (psi) : 400,000
Fibre modulus (psi) : 12,000,000

Resin radius (inch) : 0.04
Fibre radius (inch) : 0.0004

Resin poisson ratio : 0.34
Fibre poisson ratio : 0.20

Ambient temperature (^{o}C) : 20
Cure temperature (^{o}C) :150

Resin linear expansion coefficient ($^{o}C^{-1}$) : 0.00006

Fibre linear expansion coefficient ($^{o}C^{-1}$) : 0.000005

The presence of stress in fibres may be detected by examination under crossed polars. Figure 43 shows glass and carbon fibres and their associated stress fields. In glass fibres the stress provides a measure of the ability of the interface to transfer resin shrinkage stresses from resin to fibre. With carbon fibres, this measurement is not possible and it is the large stresses in the resin adjacent to fibre ends which are monitored in order to obtain evidence of debonding, see Wyatt and Ashbee (1969).[23] Once the interfacial bond is destroyed, resin shrinkage gives rise to a situation in which the fibre acts as a rigid indentor. As a consequence the stresses at the fibre ends increase.

For silane covered glass fibres debonding is either preceded or accompanied by the formation of surface bubbles, see figure 44a That these are pressure filled is evident from a comparison of the stress field of figure 44c with that of figure 44b Glass fibres contain a small percentage of alkali metal oxides; 0.6 weight % in 'E' glass. When water

reaches the interface it will readily dissolve such impurities and create an osmotic pressure (see section 3.2.4). In uncoated glass fibre specimens, such pressure will rapidly debond along the whole fibre length. When a silane coupling agent has been applied to the fibres, the increased bond strength resists this type of debonding. However bubbles still form on the glass surface in areas of incomplete silane protection and these eventually coalesce to give complete debonding. Once the interface has been wetted, it can be shown that there is a thermodynamic driving force to displace resin from it. (Gledhill and Kinloch (1976)).[24] The reversible work of adhesion, W_A, between glass and resin is given by

$$W_A = \gamma_R + \gamma_G - \gamma_{RG}$$

where γ_R and γ_G are the surface free energies of resin and glass respectively and γ_{RG} is the interfacial free energy. In the presence of a wetting liquid (denoted by the suffix 'L') the work of adhesion, W_{AL}, becomes

$$W_{AL} = \gamma_{RL} + \gamma_{GL} - \gamma_{RG}$$

The values of W_A and W_{AL} determine the stability of the bond. The surface energy terms may be split into dispersive and polar components to give the relations

$$W_A = 2[(\gamma_R^D \gamma_G^D)^{\frac{1}{2}} + (\gamma_R^P \gamma_G^P)^{\frac{1}{2}}] \qquad \text{—— 3.2}$$

$$W_{AL} = 2[\gamma_L - (\gamma_R^D \gamma_L^D)^{\frac{1}{2}} - (\gamma_R^P \gamma_L^P)^{\frac{1}{2}} - (\gamma_G^D \gamma_L^D)^{\frac{1}{2}}$$

$$- (\gamma_G^P \gamma_L^P)^{\frac{1}{2}} + (\gamma_R^D \gamma_G^D)^{\frac{1}{2}} + (\gamma_R^P \gamma_G^P)^{\frac{1}{2}}] \qquad \text{— 3.3}$$

where the superscripts D and P denote dispersive and polar components respectively. These formulae are derived in Kaelble and Uy (1970)[25] and Kinloch et al. (1975).[26] Values for materials of interest here are shown in table 8. When substituted into equations 3.2 and 3.3 the calculation yields $W_A = 178$ mJ/m^2 and $W_{AL} = -57$ mJ/m^2. This indicates that the bond is stable in a normal dry environment having a high positive work of adhesion. In the presence of water the bond becomes unstable, as indicated by the negative work of adhesion, and it is energetically favourable for the bond to be destroyed. 'E' glass has an estimated surface energy of

425 mJ/m^2 which implies increased stability of the bond when dry and instability when wet, compared to silica. In carbon fibre composites there is no wetting and, therefore, no thermodynamic driving force for debonding but there may be a situation in which impurities on the fibre surface (either organic or inorganic) provide sites for water attack.

Table 8. Surface energies

Solid Surface	λ^D	λ^P (in mJ/m^2)
Epoxy resin	41.2	5.0
Silica	78	209
Water	22.0	50.2

4. CONTINUING RESEARCH

The understanding gained of the characteristics peculiar to epoxy resins making them susceptible to water attack, would suggest that a more chemically pure resin, in which no manufacturing residues remain, would lead to improved and extended service. Probably less expensive and easier to control would be thorough characterisation of resins, in particular a search for precise stoichiometric mix proportions and efficient cure schedules. This would make feasible the achievement of complete reaction and a truly homogeneous and amorphous resin matrix. The problem of avoiding anomalous surface layers is more difficult. However, the possible advantages of curing in an inert atmosphere and casting in an inert mould may well be worth examination. Interfacial anomalies in composites or joints is believed to be unavoidable since the bonding relies on interfacial attractions. These will not be identical for polar and non-polar groups for example, and will result in an excess of one type of group. If the interface is designed to be weak, it is important to ensure that water cannot easily attack it, and the development of better gel-coats for composites seems to be a particularly worthwhile goal.

The light-pipe technique is now established as a means of detecting interfacial changes in continuous fibre composites. As yet only small specimens have been tested but it appears that full scale tests will be simpler to carry out. For example, at present one of the main sources of inconsistency and light intensity loss is the introduction of light into a small specimen. A larger resin structure would incorporate a fixed input recess to which a light source could be attached unambiguously. The detector photocell would be cast into the structure and if this were done, external conditions would no longer influence

measurements. Attenuation in the fibres is negligible and the use of a larger specimen should not affect the sensitivity of the method.

An attempt will be made to use optical interference methods to map the elastic deformation of a glass wafer during bonding to a slab of epoxy resin that is rigidly supported on its other side. If successful, the experiment will be repeated for deformations resulting from resin swelling during water uptake and for deformations in the presence of coupling agents. Calculation of the distribution of stress corresponding to these deformations is expected to provide insight into the phenomenon of enhanced water uptake by resin/glass interfaces.

More details of each of the above areas of work are contained in N. R. Farrar's Ph. D. thesis which will shortly become available.

Development work on the ultrasound equipment will continue and data from composites and bonded and debonded resin/glass interfaces will be collected. It will shortly be possible to calculate the elastic constants of any opaque block, and as development proceeds, it is likely that the 'intelligence' carried by the wave trains will yield more data. Debonding at an interface should be 'observed' ultrasonically, for example. However, it is important to strike the correct balance between stress wave frequency and attenuation in the media involved. Higher frequencies give more information, but also give greater attenuation. Nevertheless the results already obtained have been encouraging.

While the electronic control and optical arrangements have been developing experimentally, we have been considering what theoretical approach would lead to a clearer understanding of the ultrasonic visualising technique. With diffraction of the wave fronts, it was considered important to use wave theory in any mathematical modelling, leading inevitably to severe problems in all but the simplest configurations.

We have now found that a simple model in two dimensions has a good potential for an effective model at the interface. Slater, Baborovsky and Marsh (Ultrasonics International 1975 Conference Proceedings)[27] have obtained good agreement from such a model with schlieren experiments for the interaction between an ultrasonic pulse and a surface defect. We are investigating the development of the program for interfacial configurations.

Assuming that the bonding promoted by coupling agents does not depend on the modification of silica usedas fibre, it might be instructive to employ crystalline quartz fibre so that

the piezoelectric effect in the latter can be exploited in order to investigate bonding efficiencies. A pilot experiment designed to explore this idea will be launched.

Resin samples currently undergoing exposure to the atmosphere at Kano, Nigeria will be returned to England for comparison with identical samples exposed to the atmosphere in Bristol and with samples subjected to accelerated tests in the laboratory. These included samples of A2, B, C and D resin systems with and without glass and carbon fibres.

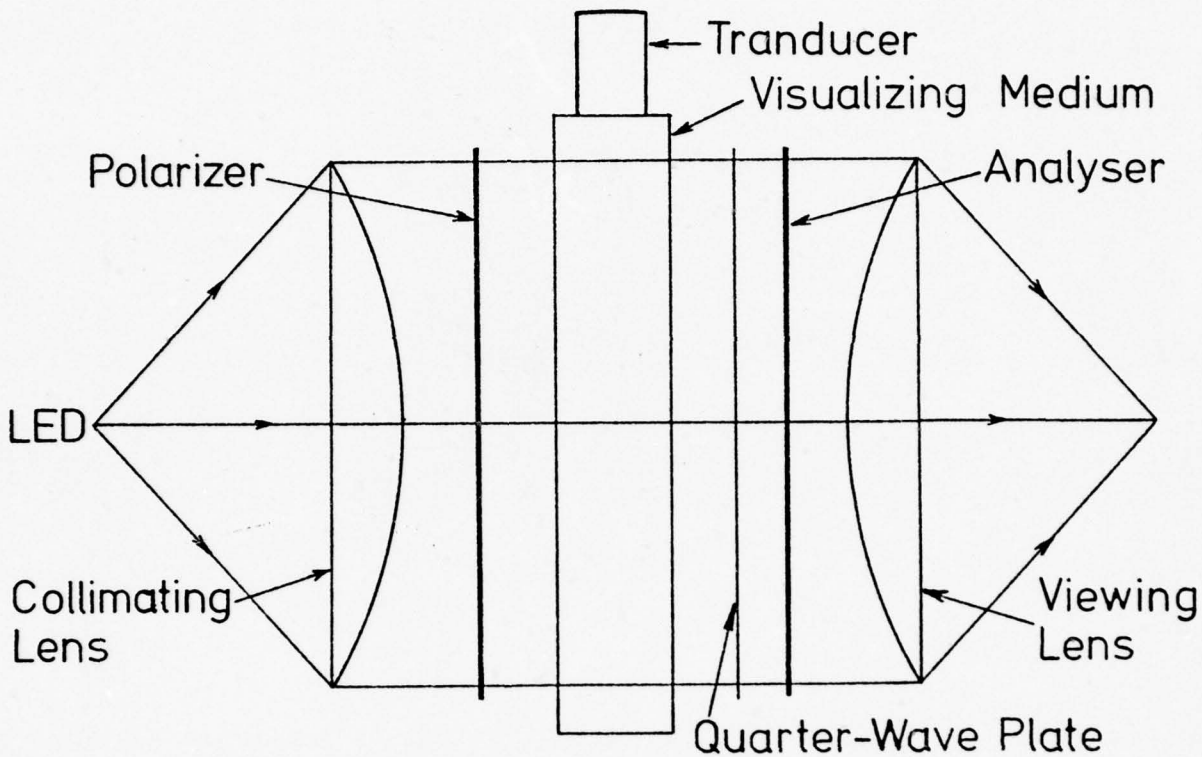

Figure 1. Principal Components of the Photoelastic Visualisation Technique.

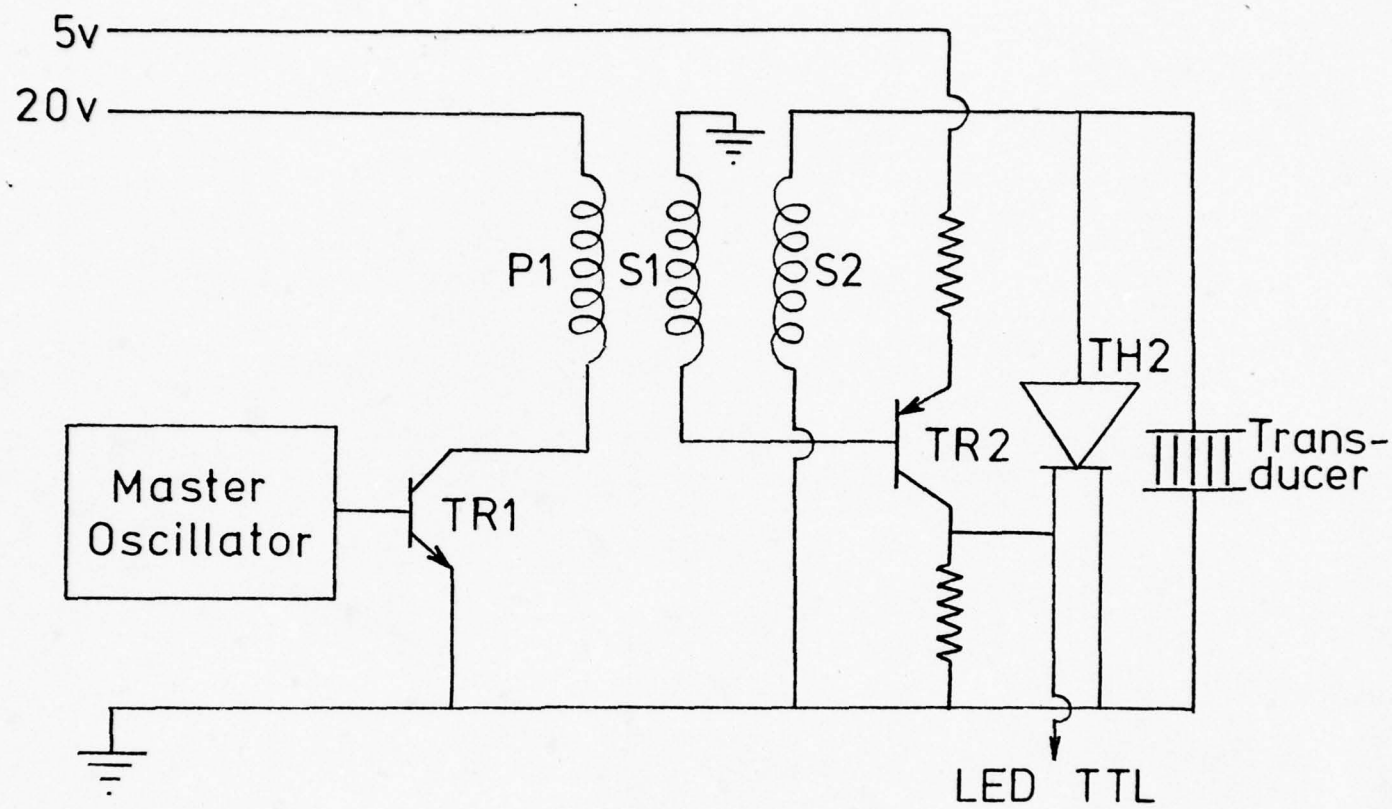

Figure 2. Ultrasonic Transducer Driver Stage.

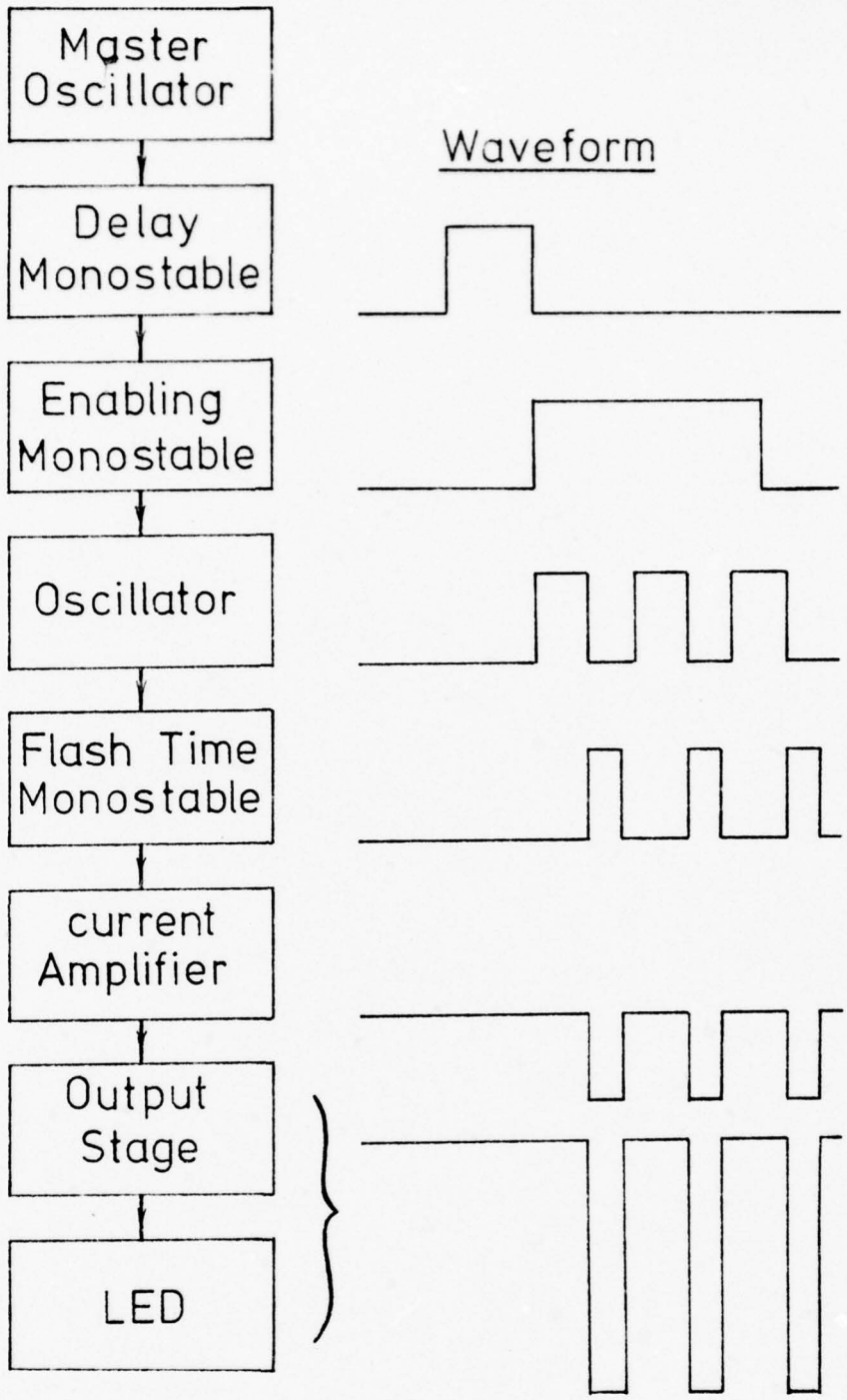

Figure 3. Block Diagram of the TTL LED Circuitry.

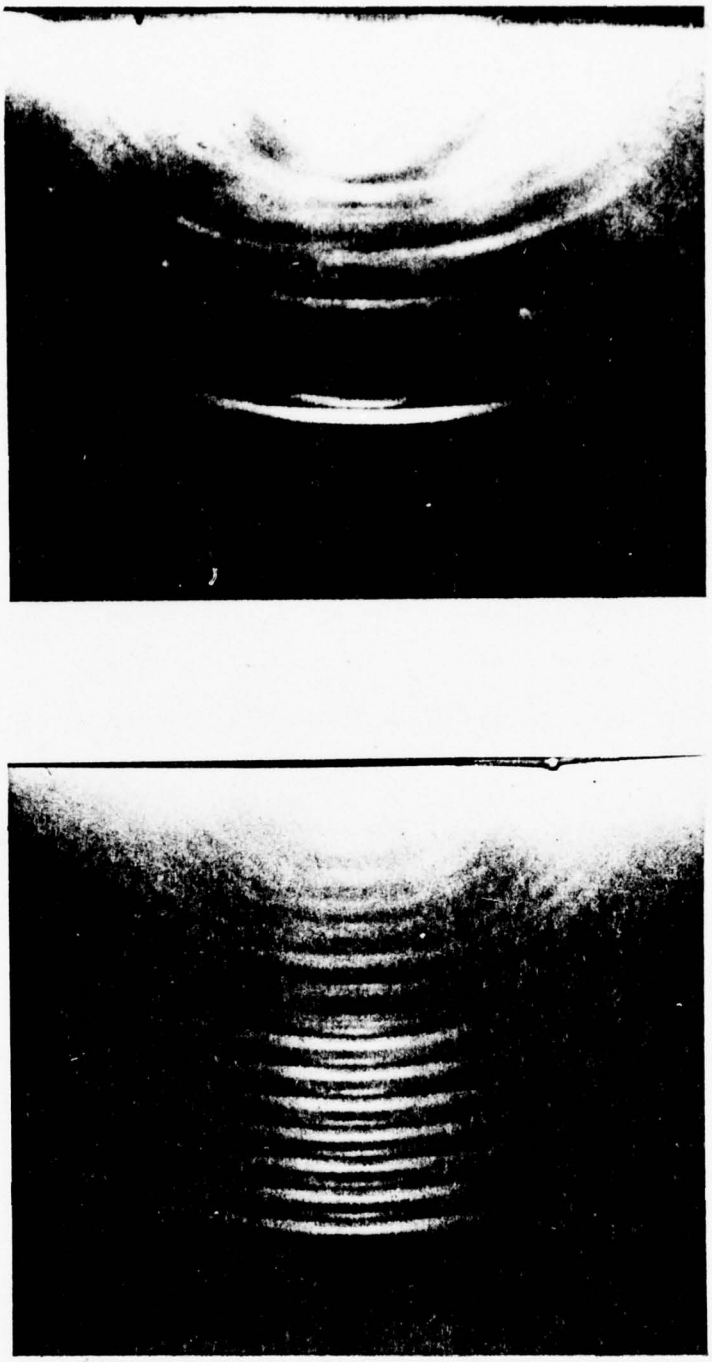

Figure 4. Single and multiple pulses in fused quarts (2 MHz)

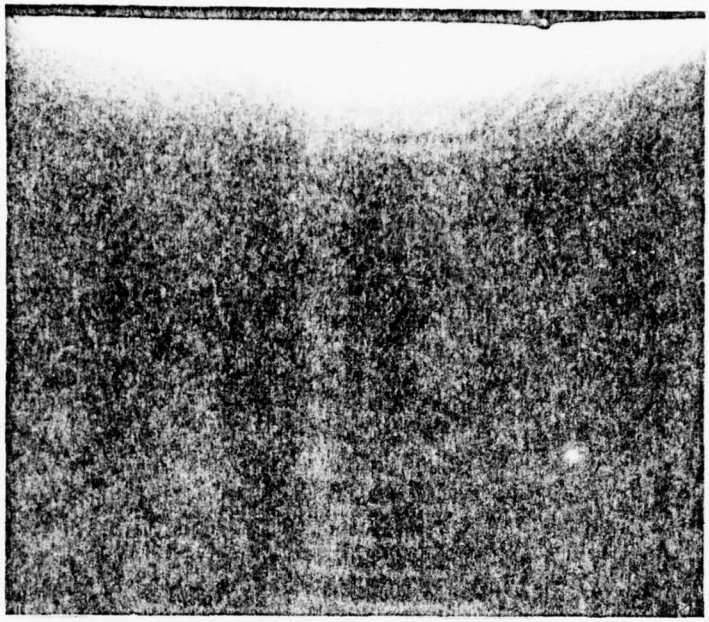

Figure 5. 2 MHz pulses after passing through steel.

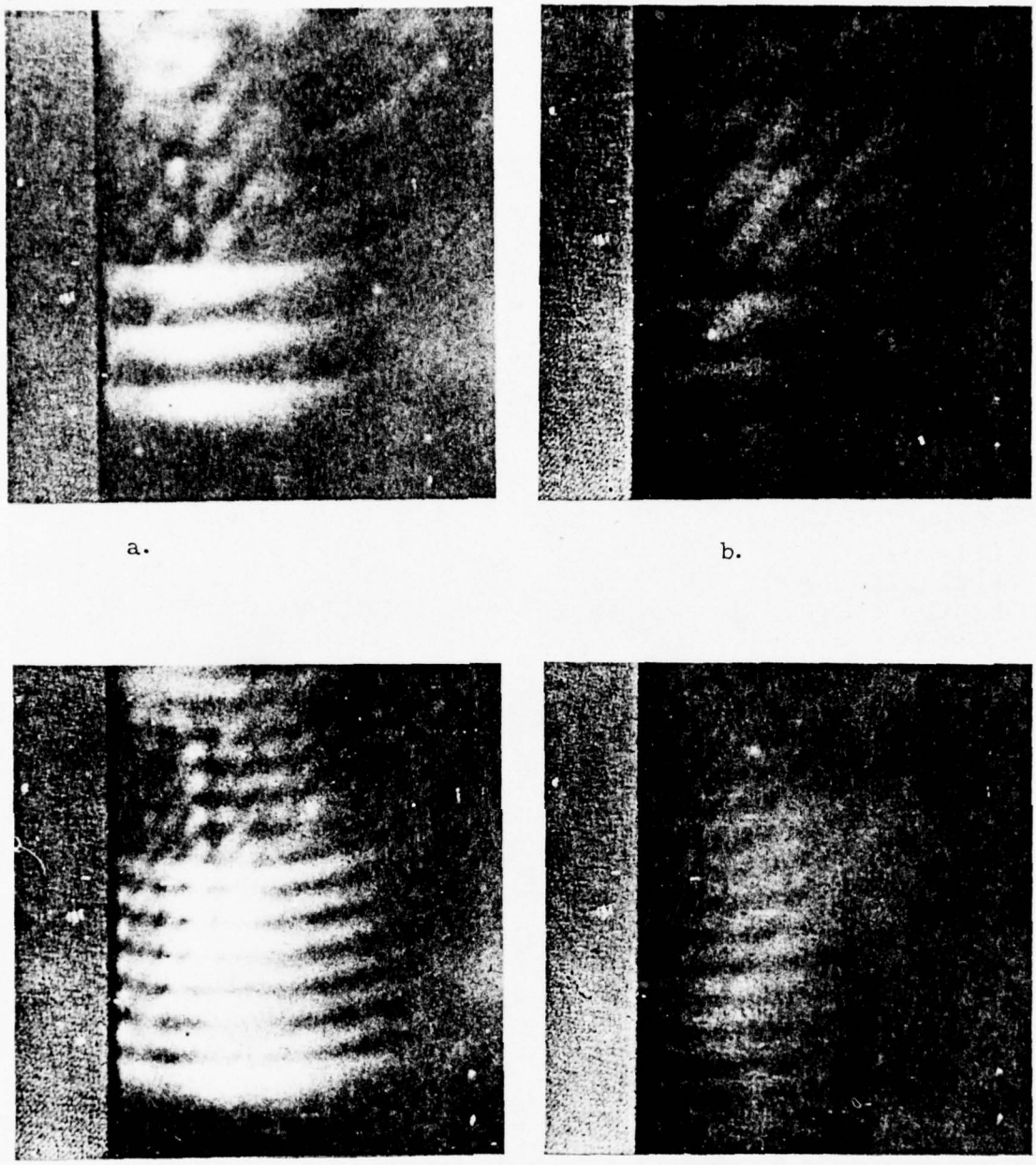

a. b.

c. d.

Figure 6.

a. 3 fringes illuminated in quartz.

b. The fringes of a. after passing through 8.35 mm of GRP composite.

c. 7 fringes illuminated in quartz.

d. The 7 fringes of c. after passing through 8.35 mm of GRP composite

Untrasonic frequency: 2 MHz, with LED flashed in synchronism.

λ_T = fringe spacing - 2.95 mm.

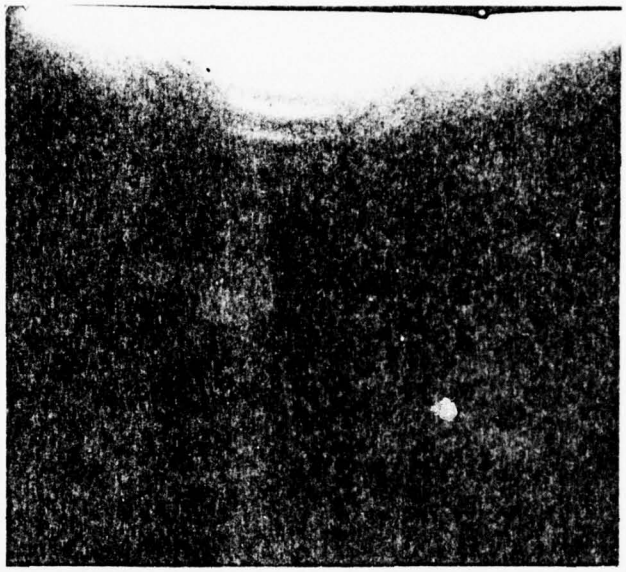

Figure 7. 2 M Hz longitudinal and shear waves.

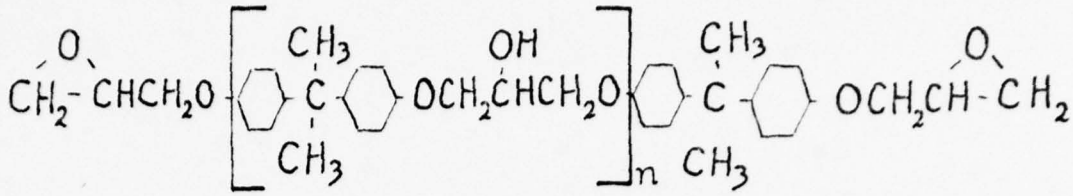

Figure 8. Ideal DGEBA structure

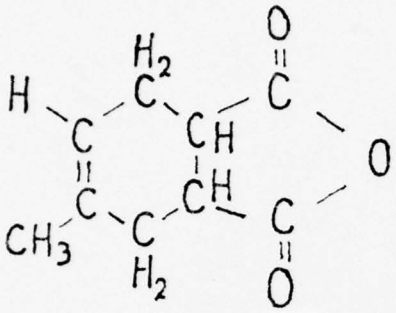

(a) Methyl tetrahydro phthalic anhydride

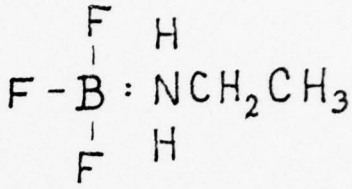

(b) Boron trifluoride: monoethylamine

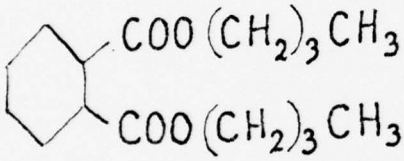

(c) Dibutyl phthalate

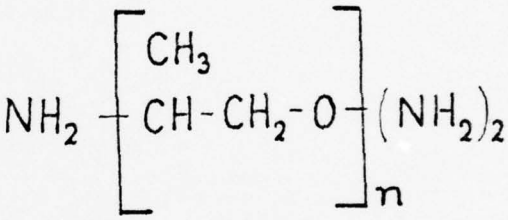

(d) Polyoxypropylene triamine

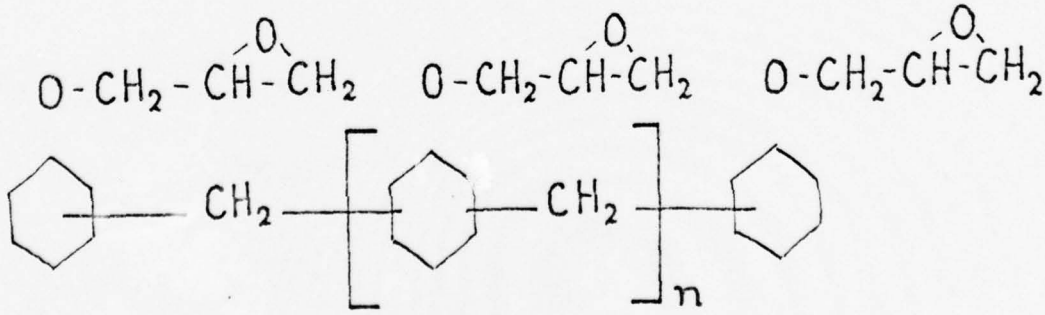

(e) Polyglycidyl ether of phenol formaldehyde novolac

Figure 9. Chemical structures of system components

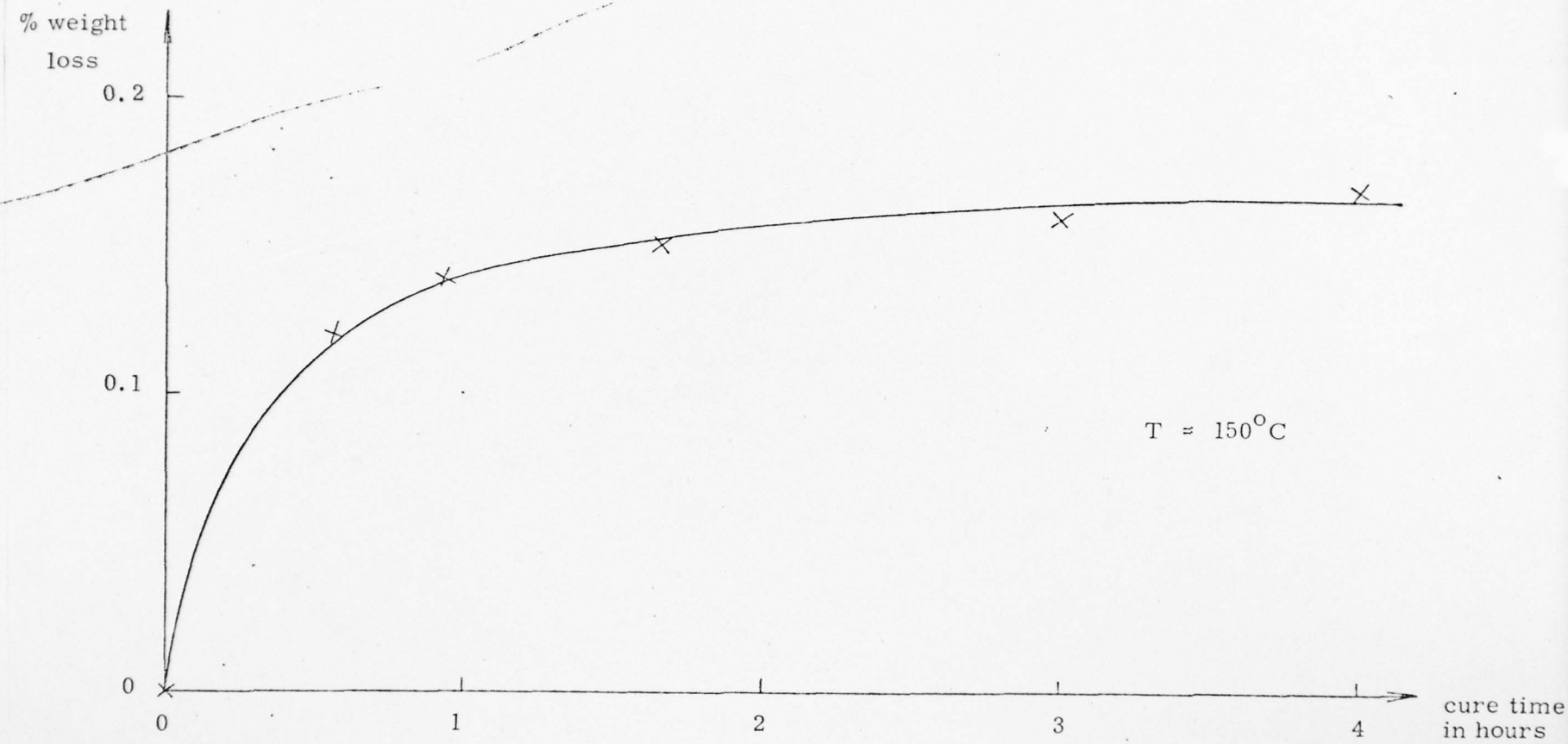

Figure 10. Weight loss with cure time for type A resin.

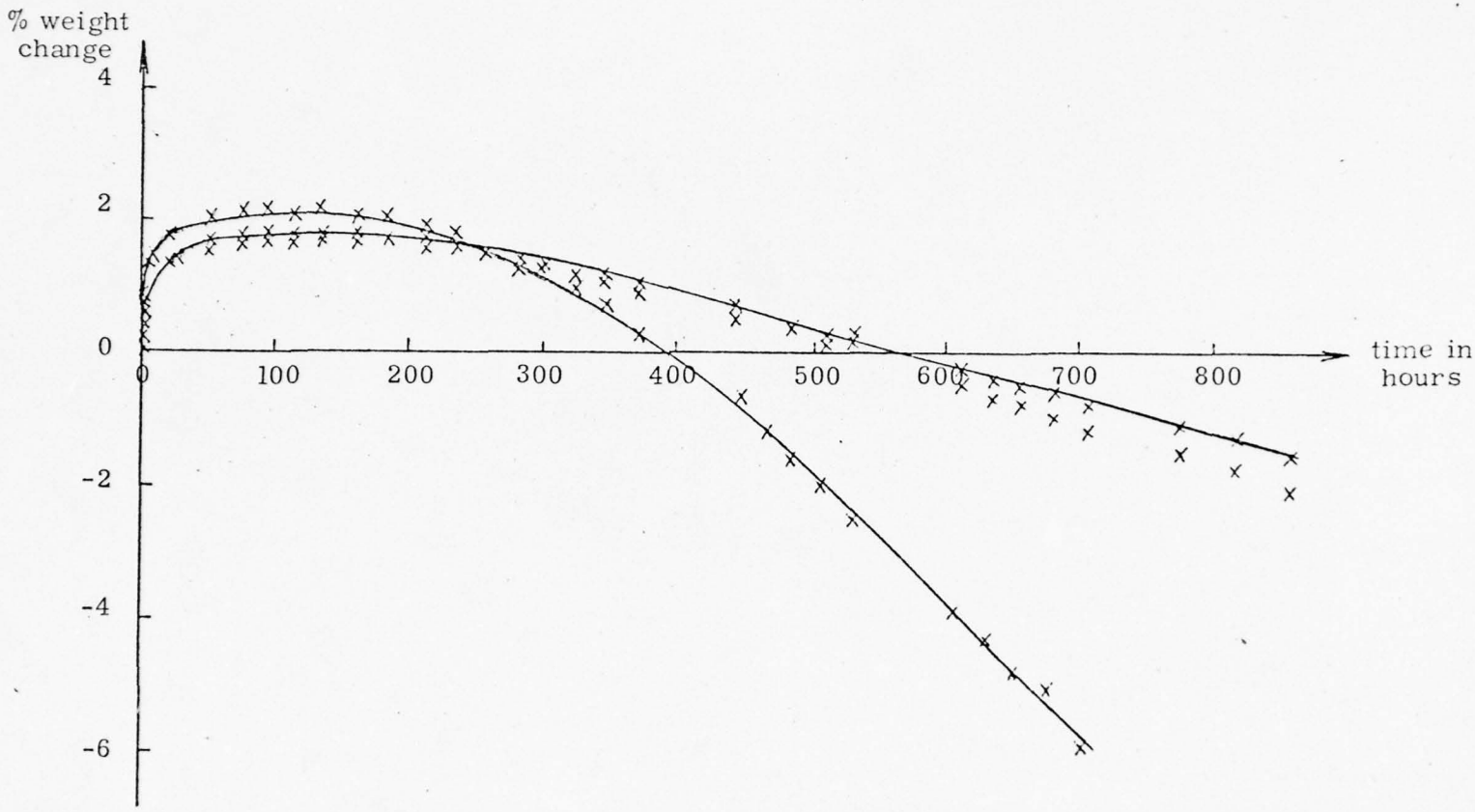

Figure 11a. Weight change against immersion time in 100°C water.

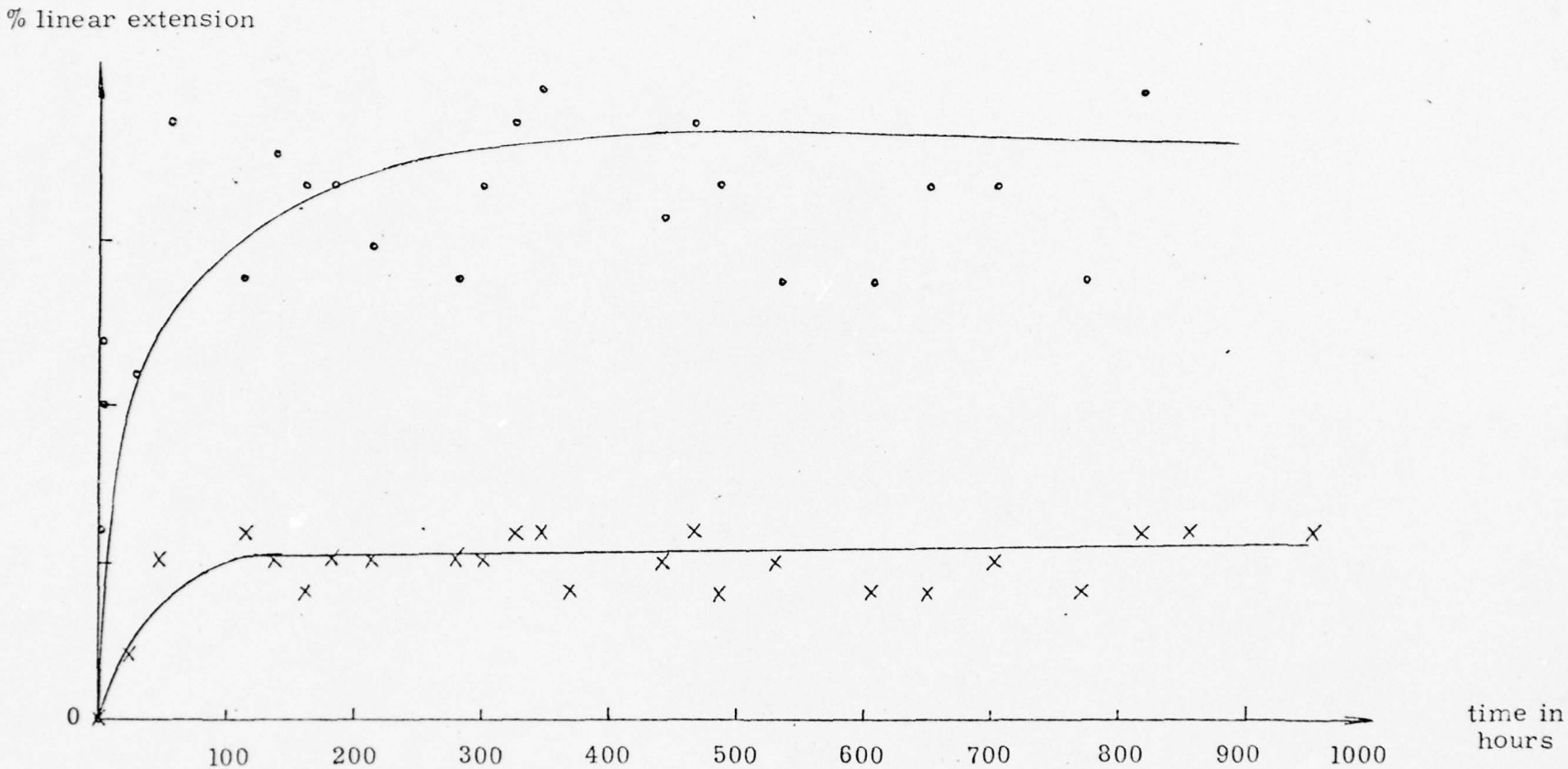

Figure 11b. Linear expansion against immersion time in 100°C water.

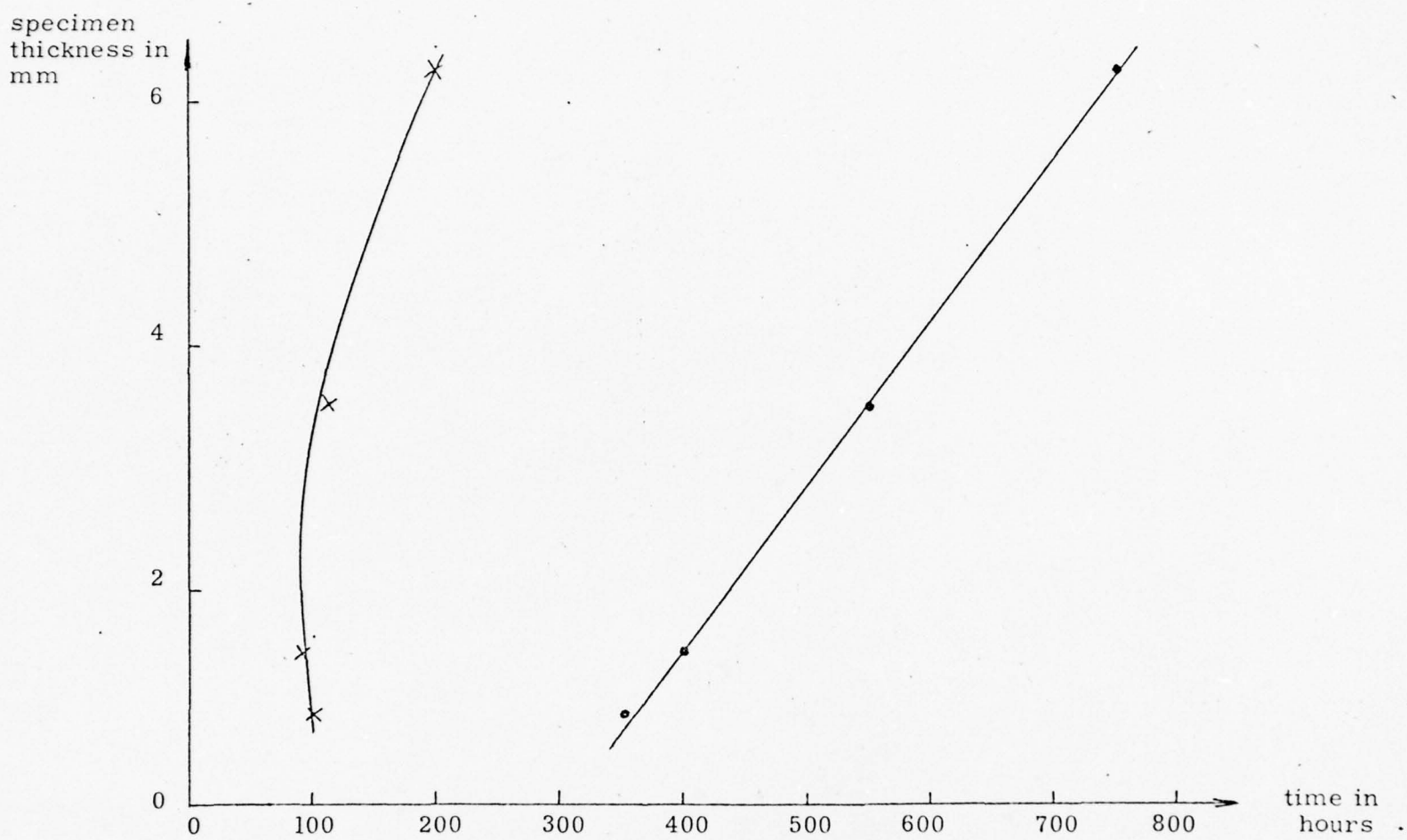

Figure 12. Variation of time to reach maximum weight (x) and time to return to original weight (•) with specimen thickness.

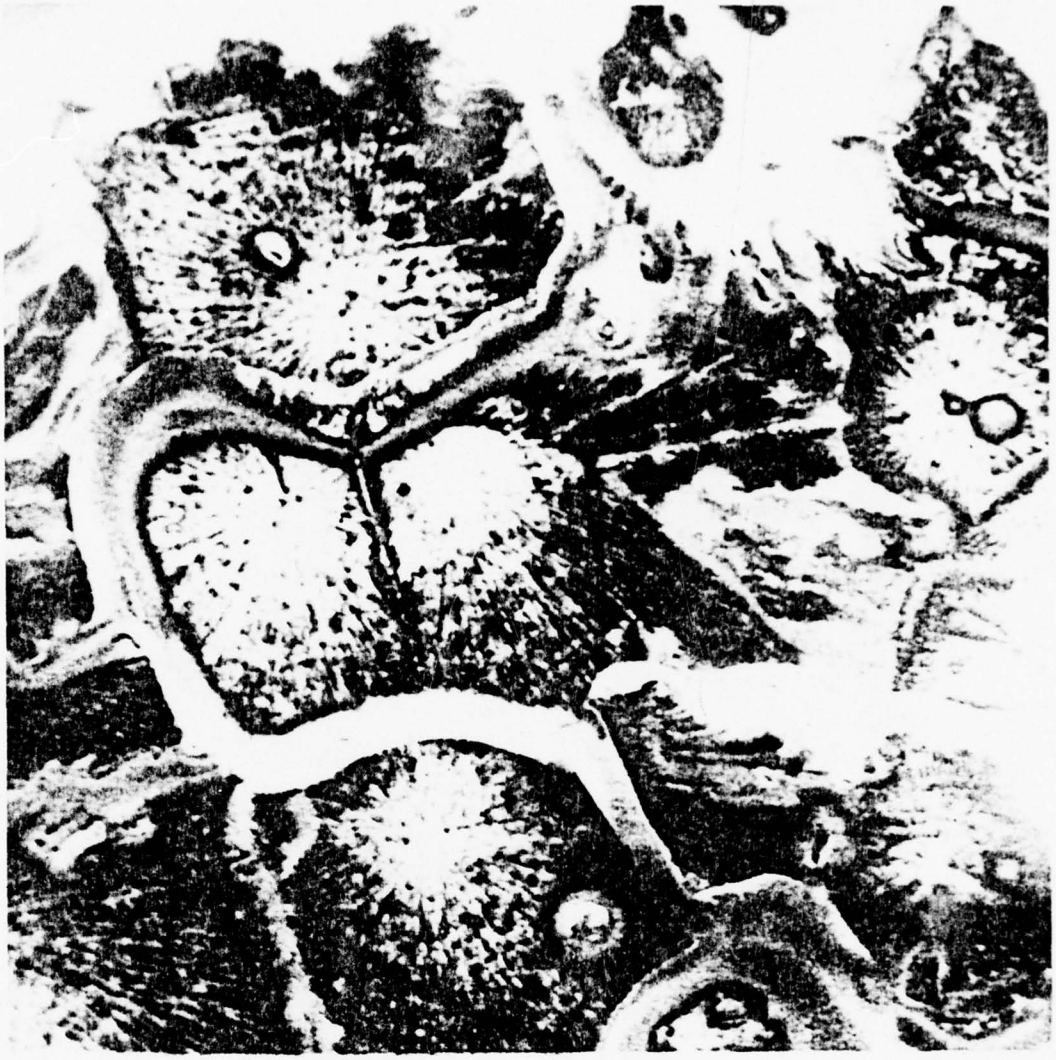

×800

Figure 13. Fracture surface to show spherulitic structure.

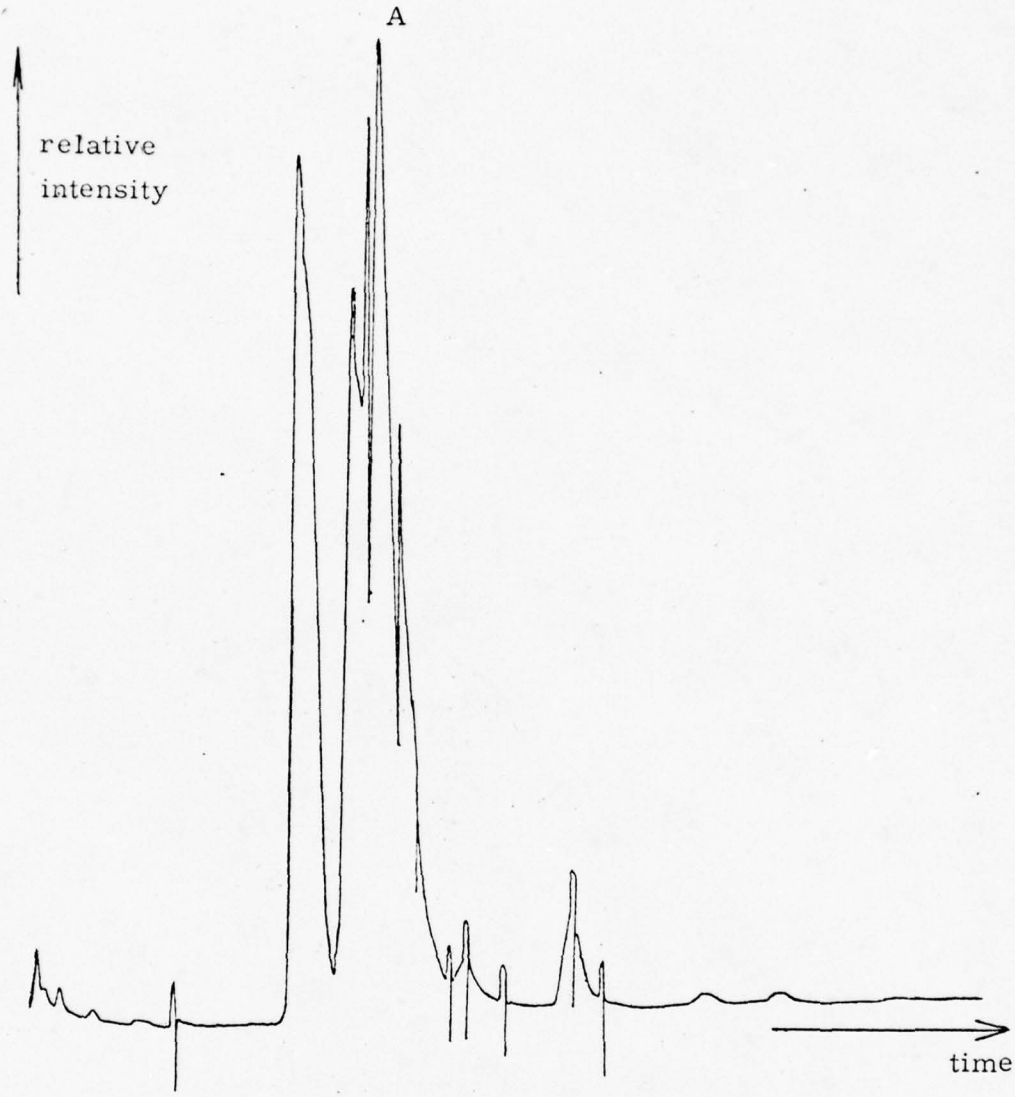

Figure 14a. Gas chromatograph total ion current (TIC) trace for 100°C immersion water.

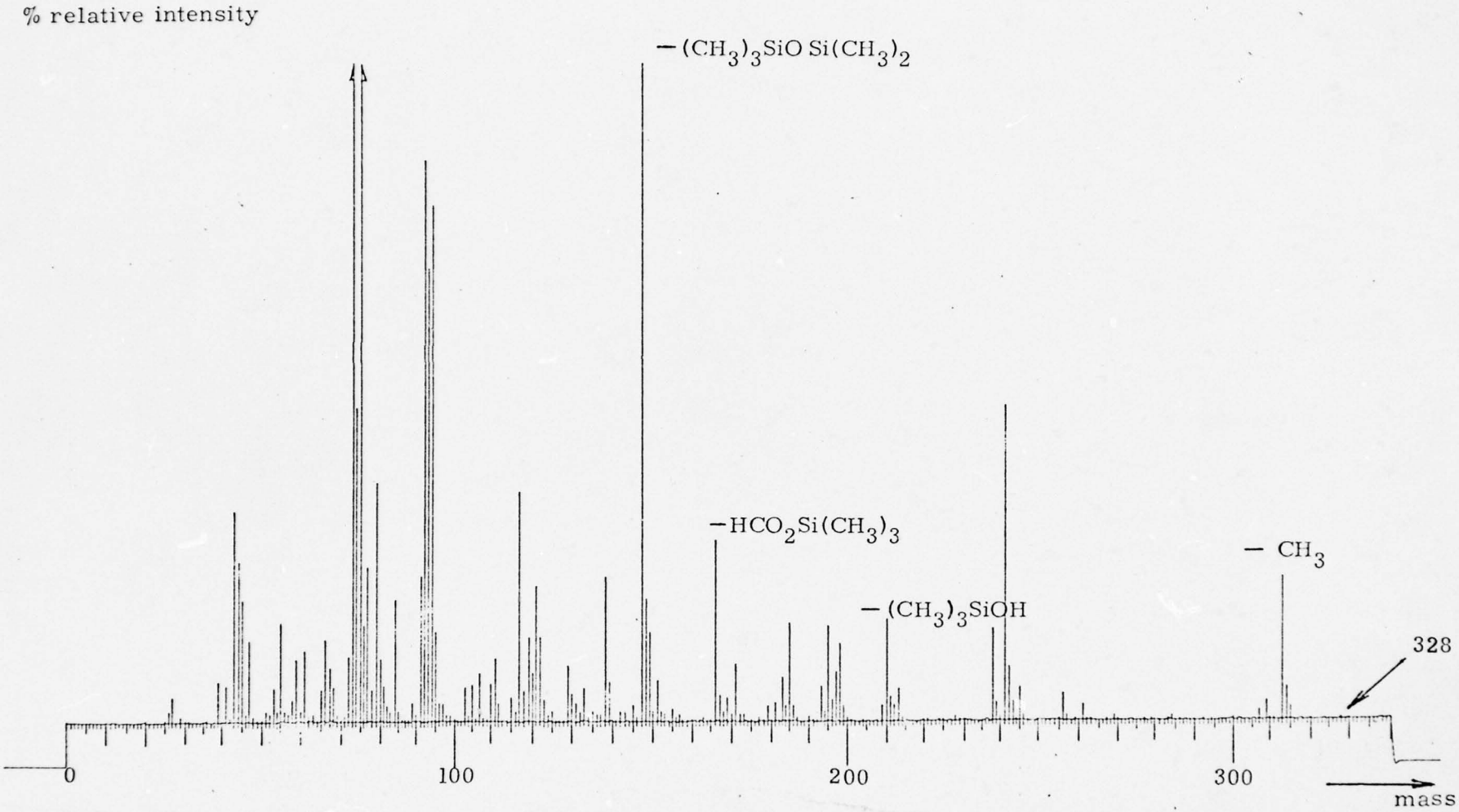

Figure 14b. Computed mass spectrum of one component of TIC.

Figure 15. Flame ionisation for (a) pure water.

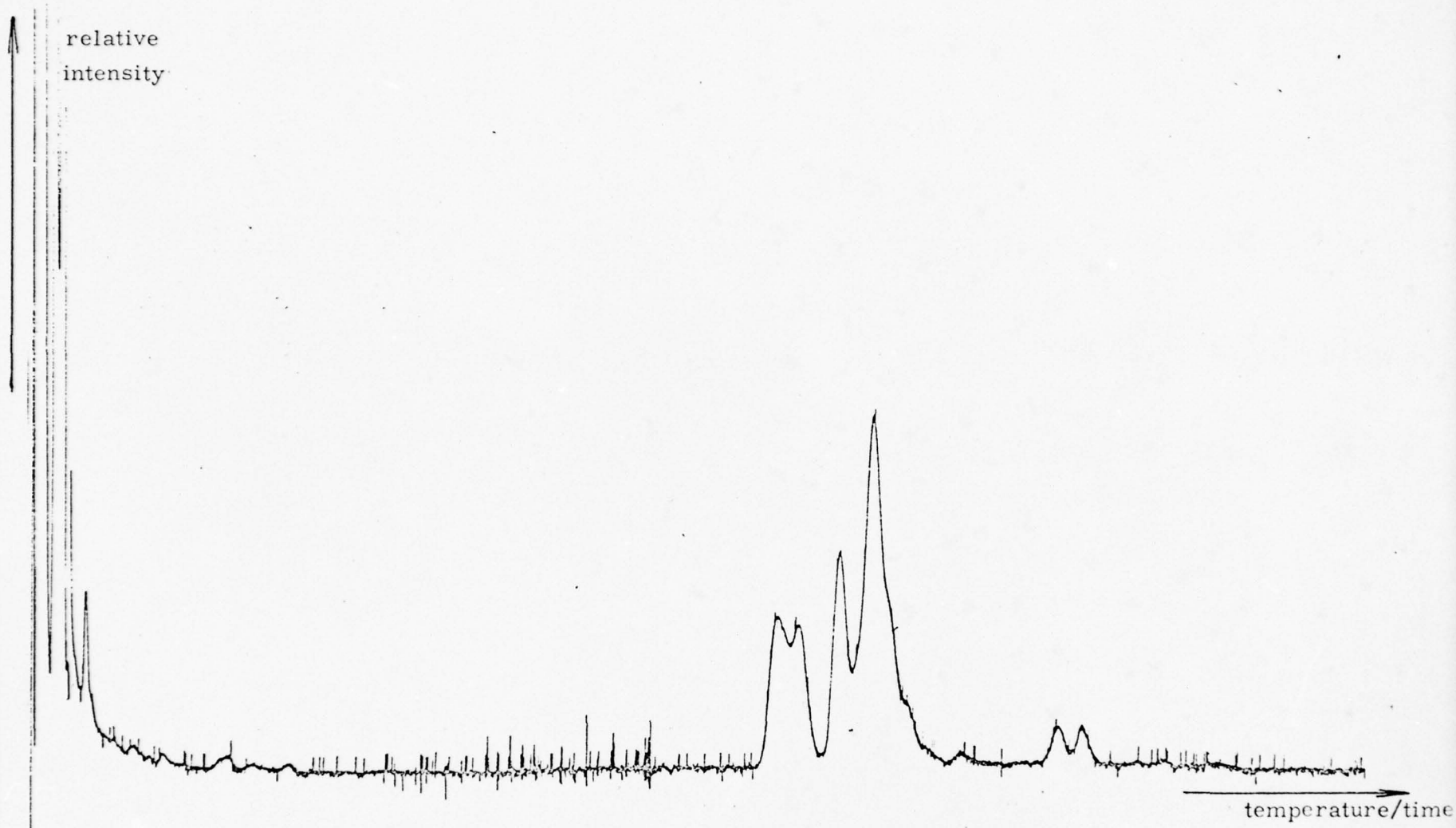

Figure 15. Flame ionisation for (b) 100°C immersion water.

Figure 16. Scanning electron micrograph of internal cracking.

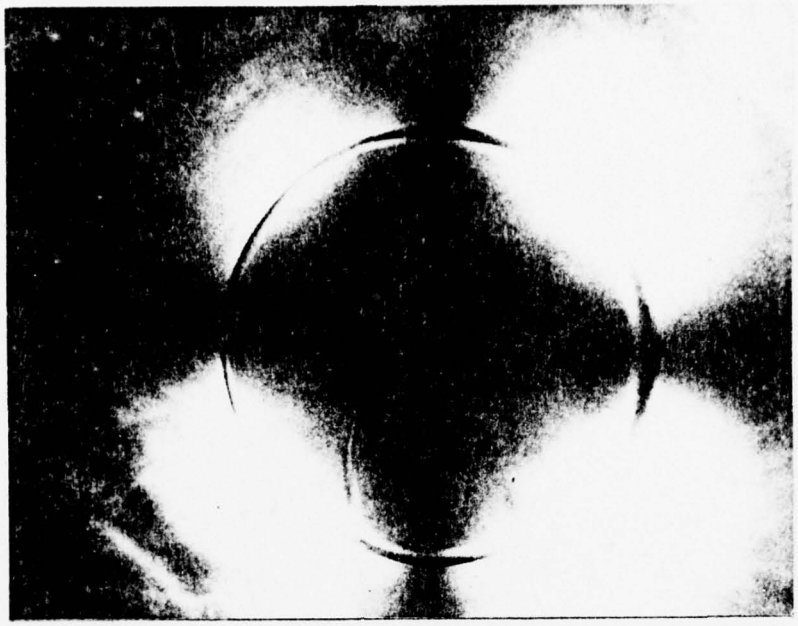

×400

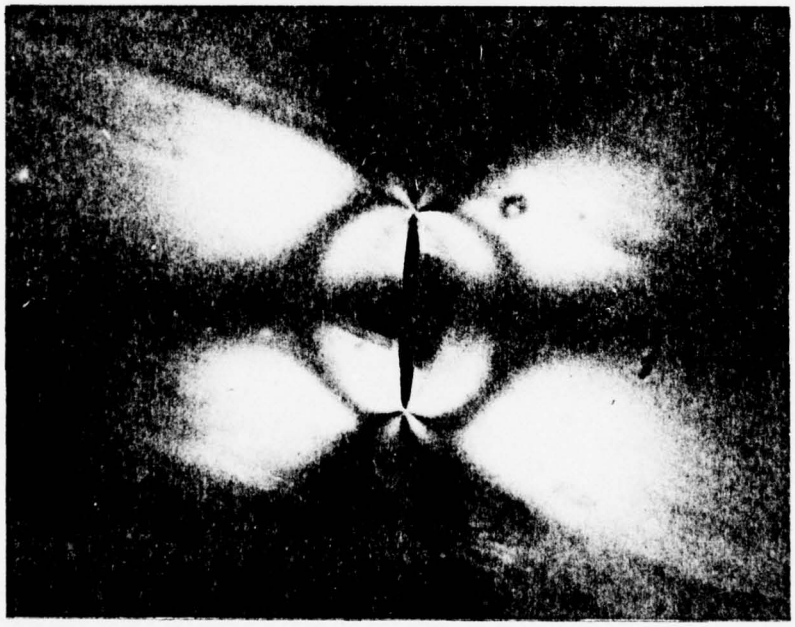

×150

Figure 17. Stress birefringence around internal cracks viewed (a) face-on and (b) edge-on.

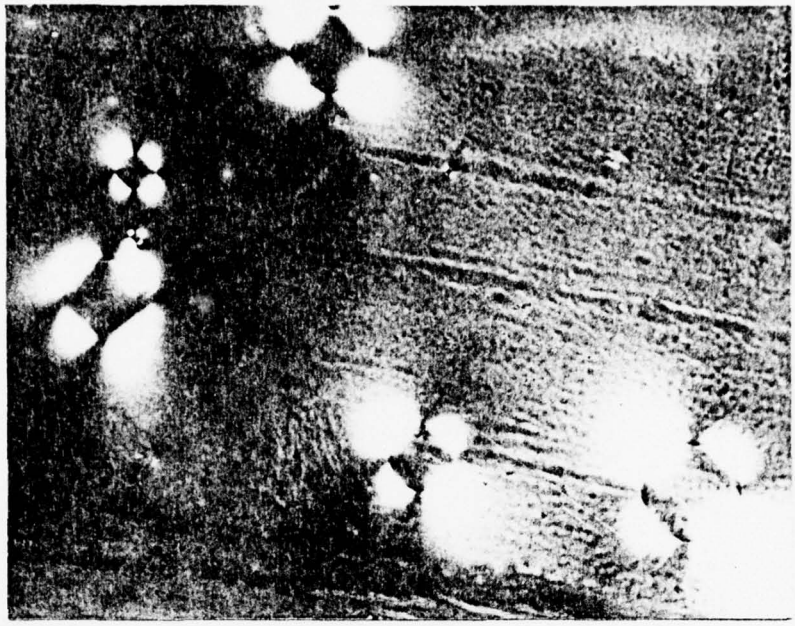

×150

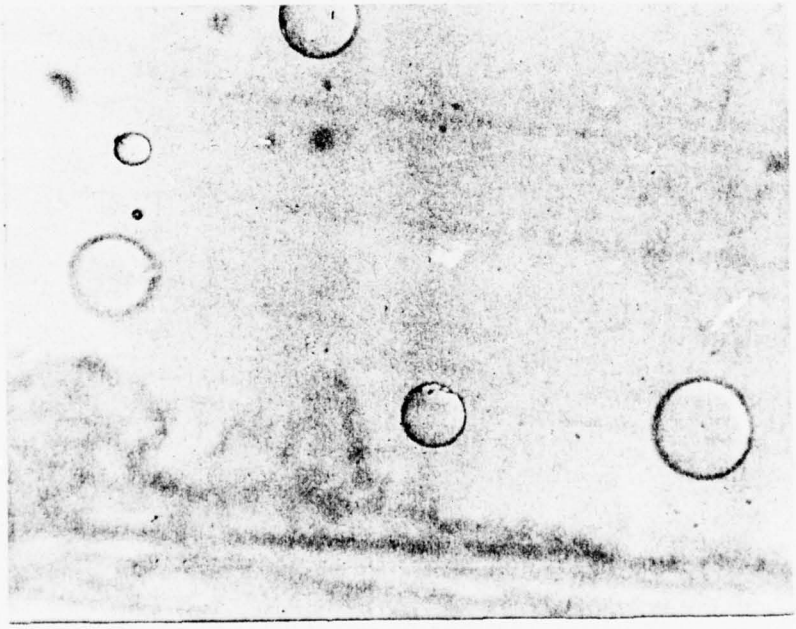

×150

Figure 18. Comparison of internal cracks viewed with and without crossed polars.

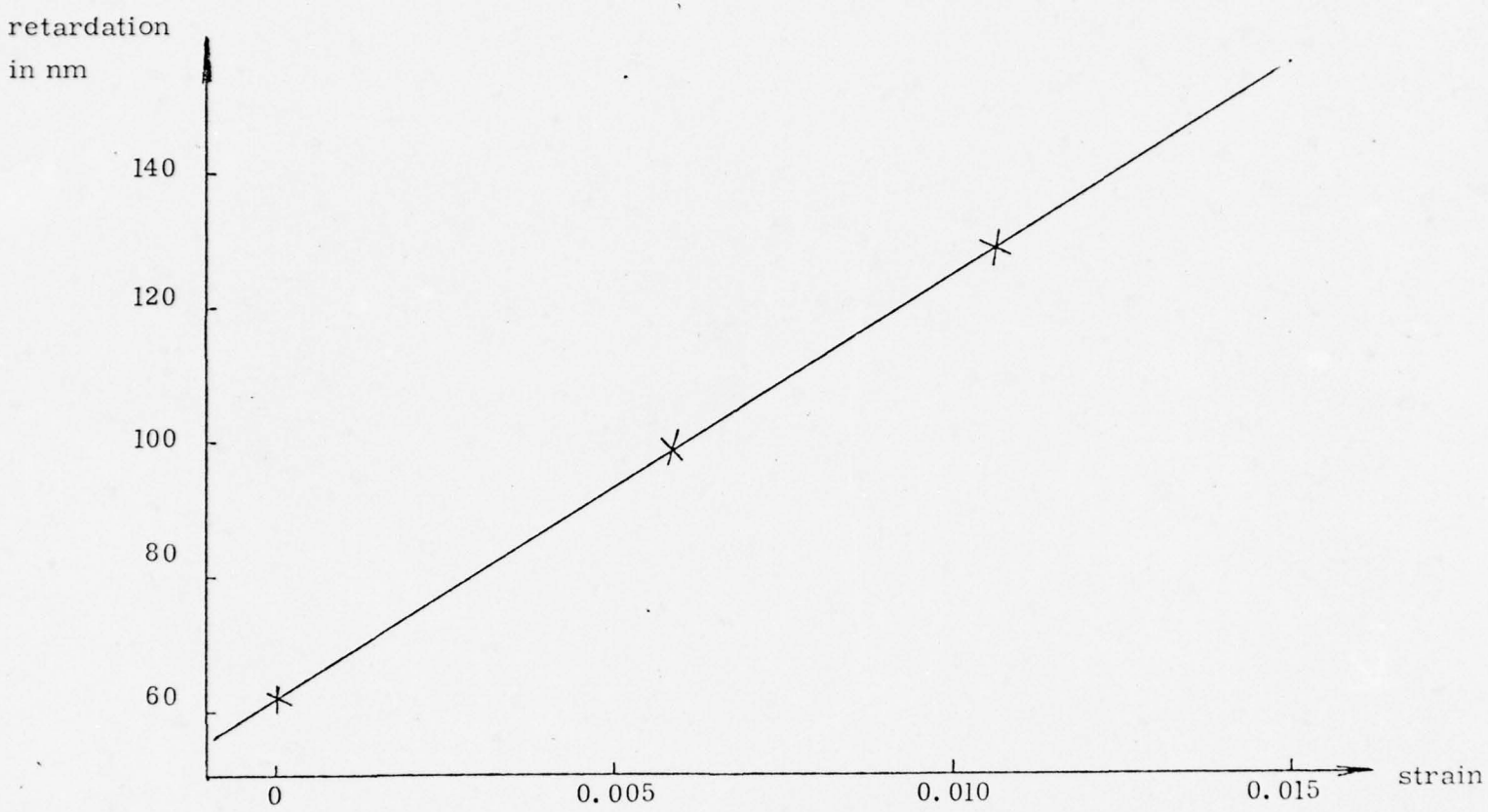

Figure 19. Variation of birefringence with strain for epoxy resin at room temperature.

×30

Figure 20. Internal cracking in resin type A.

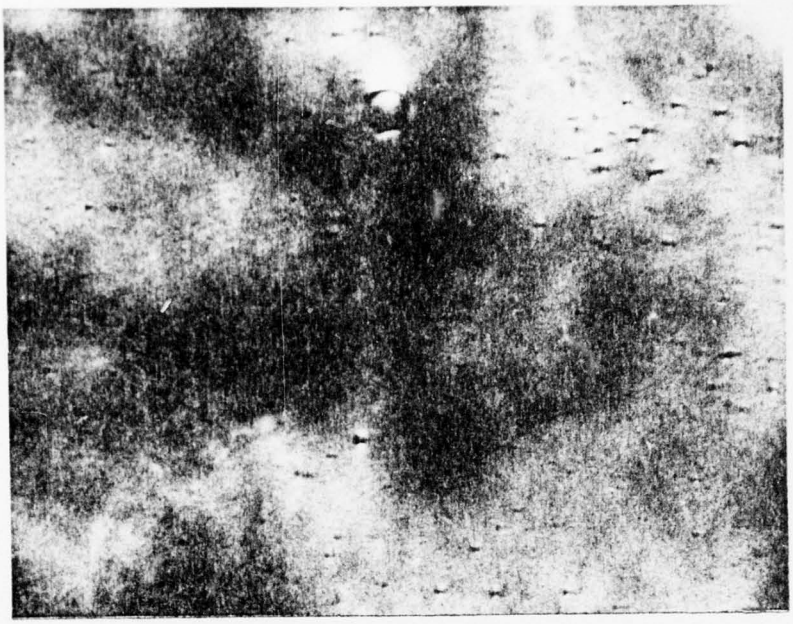

×120

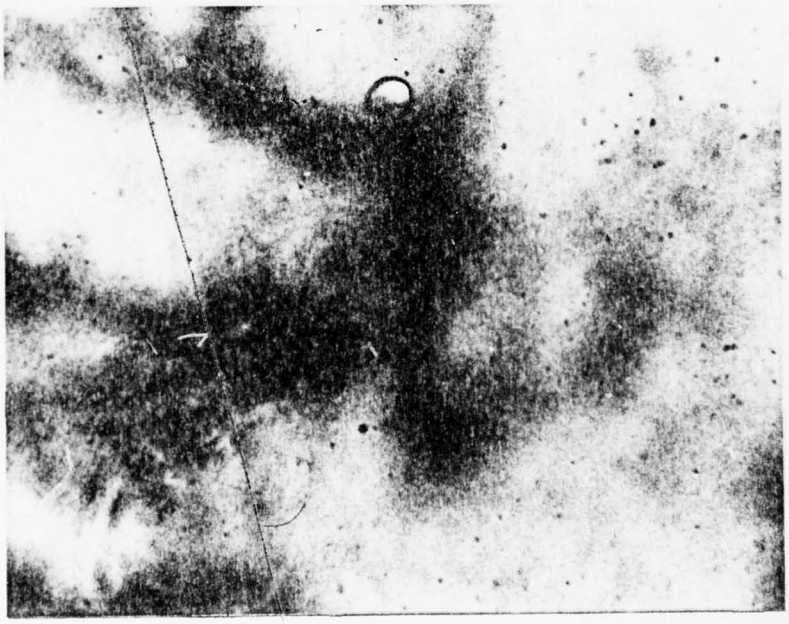

×120

Figure 21. Internal cracking in resin type C.

Figure 22. ×250

Cracking of resin type C viewed through crossed polars.

×250

Figure 23. Internal cracking around an impurity inclusion.

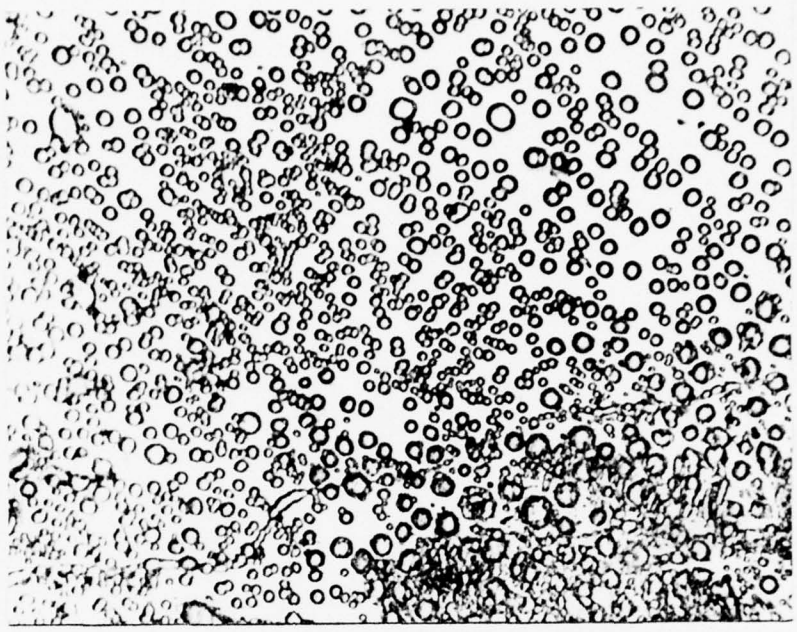

×250

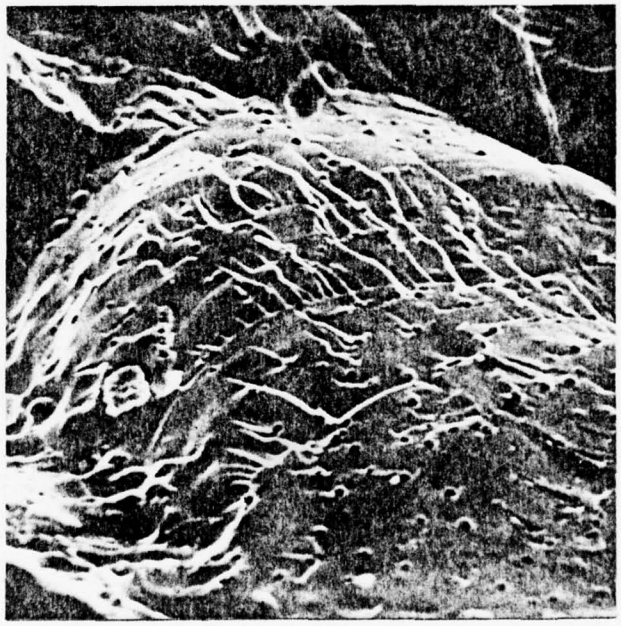

×500

Figure 24. Optical and electron micrograph of spherical cracking.

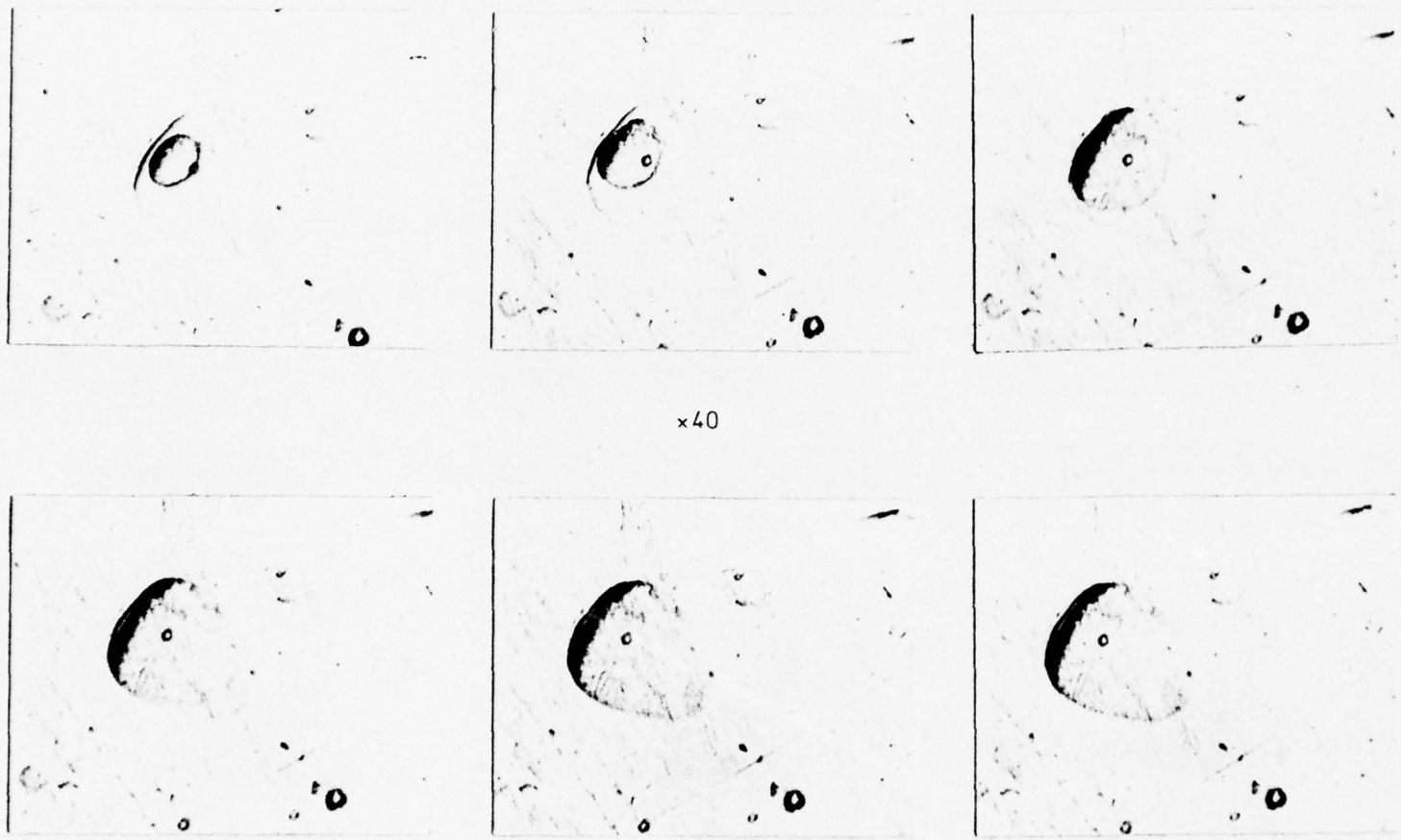

Figure 25. Sequence showing growth of air bubble in an internal crack after removal from water.

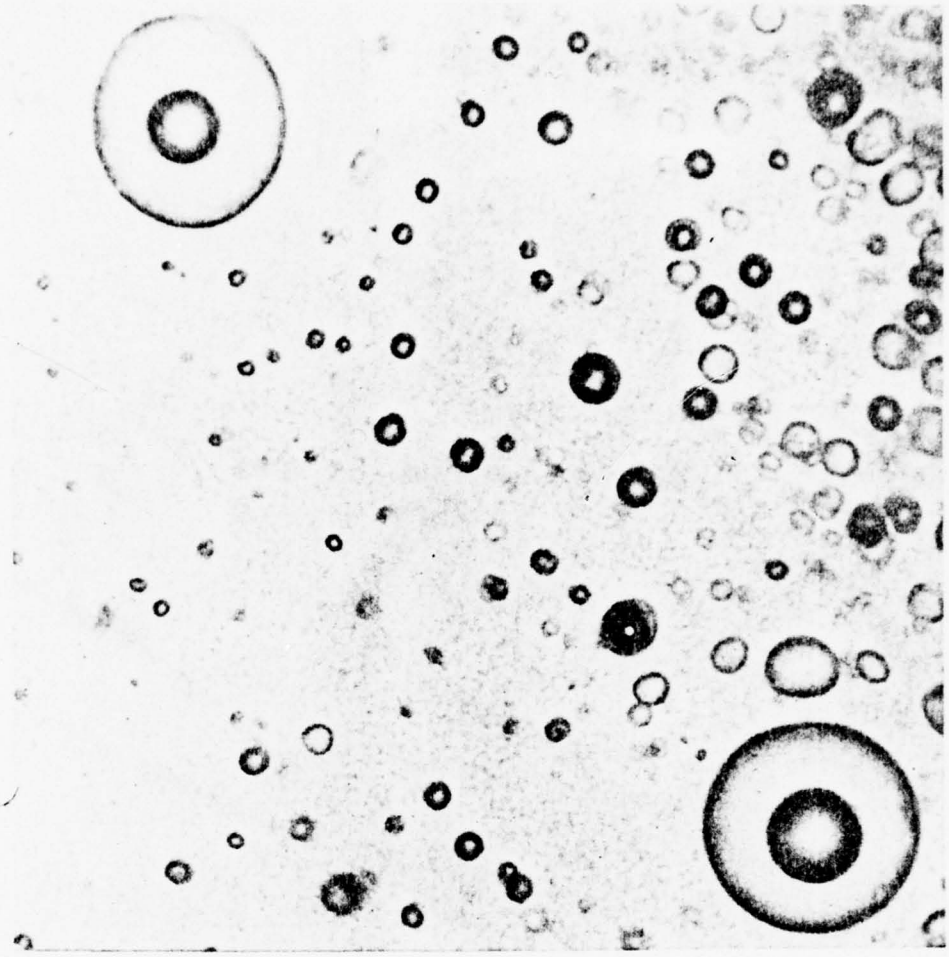

×400

Figure 26. Air bubbles in internal cracks.

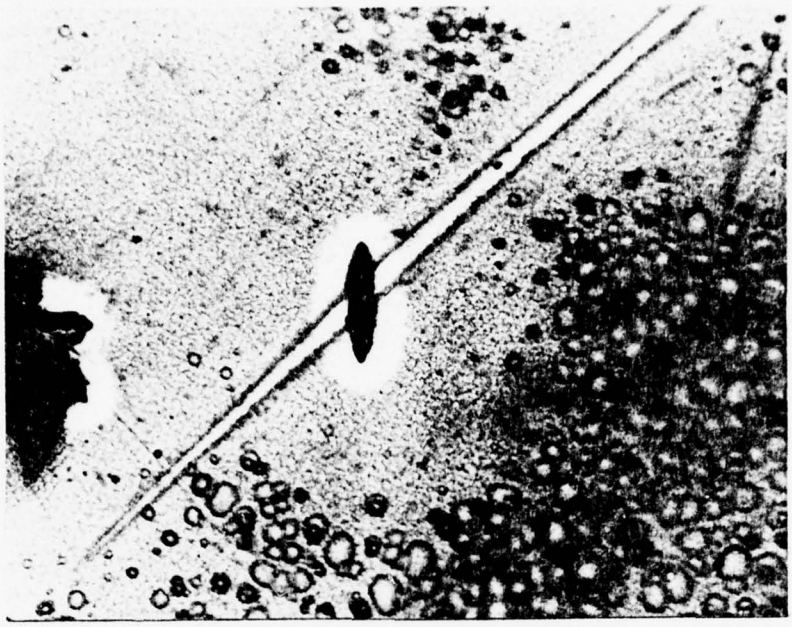

×150

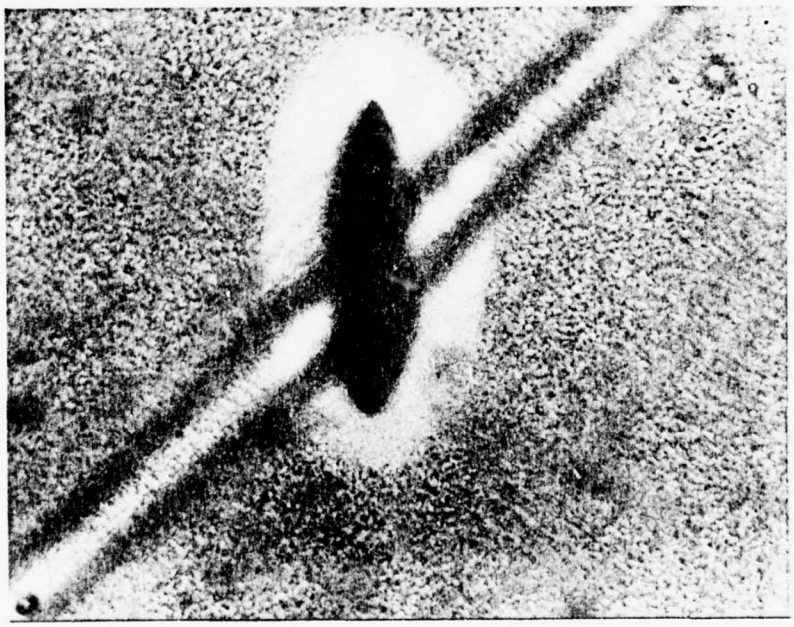

×350

Figure 27. Condensed water around an internal crack.

×100

Figure 28. Condensed water around cracks.

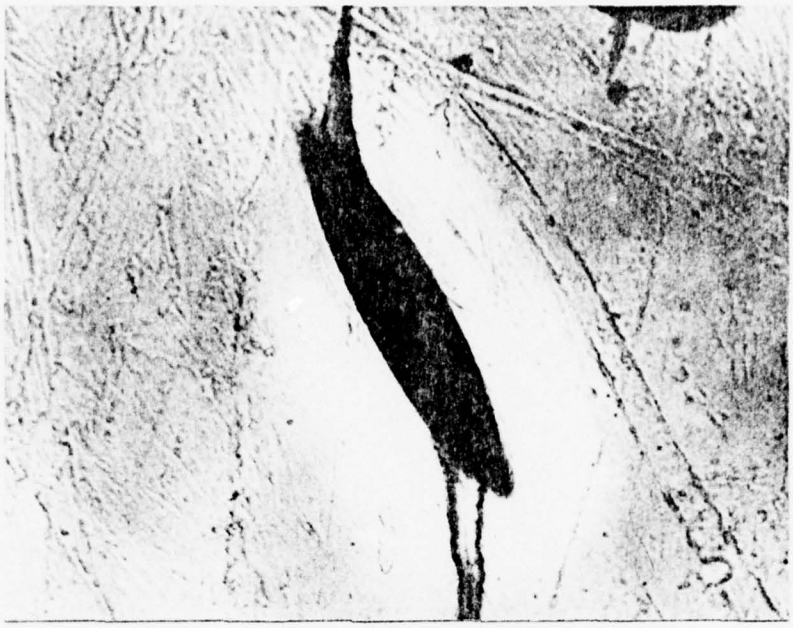

×350

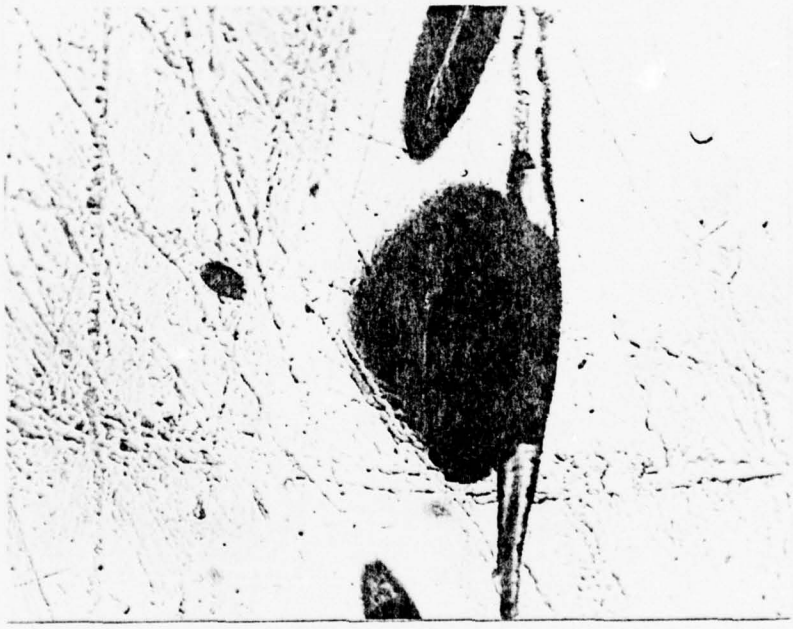

×350

Figure 29. 'Wormholes' growing from internal cracks.

Figure 30a.

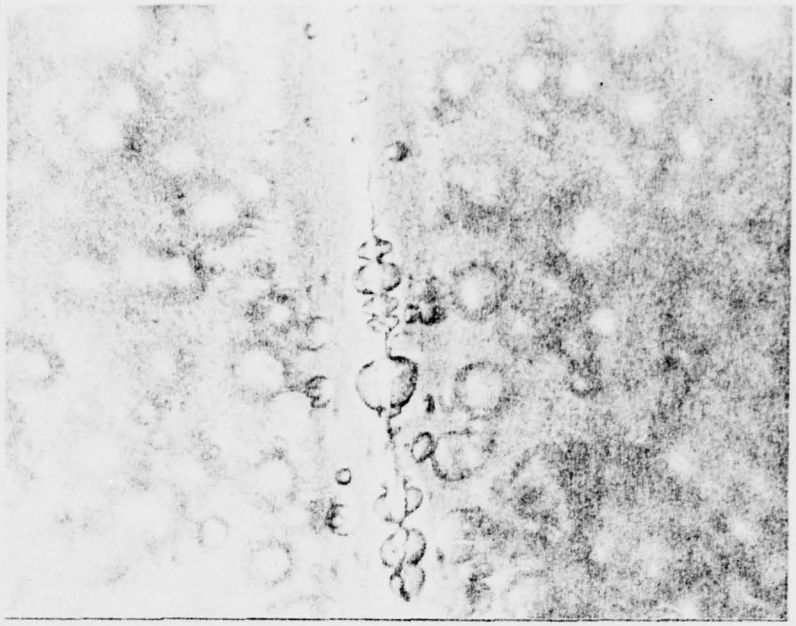

×350

×350

Figure 30b. Internal structures of 'wormholes'.

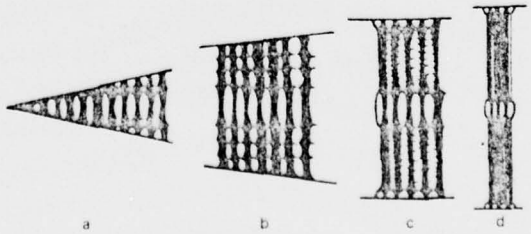

Figure 30c. Model for craze production (after Beahan et al. (1972))[19]

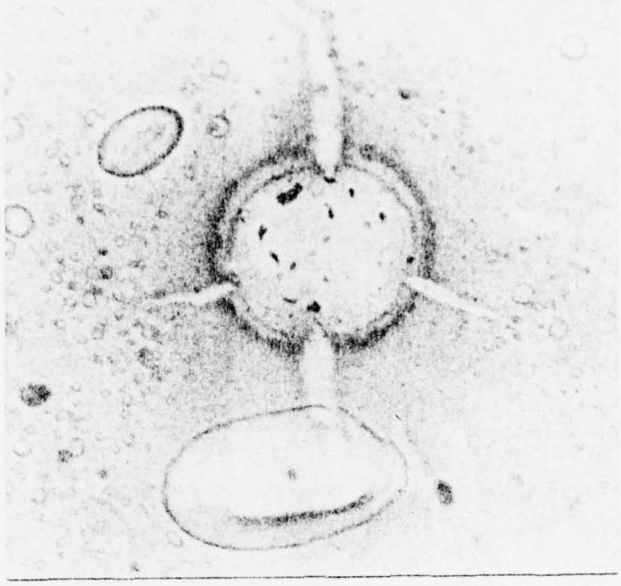

×350

Figure 31a. Impurities visible in face-on cracks.

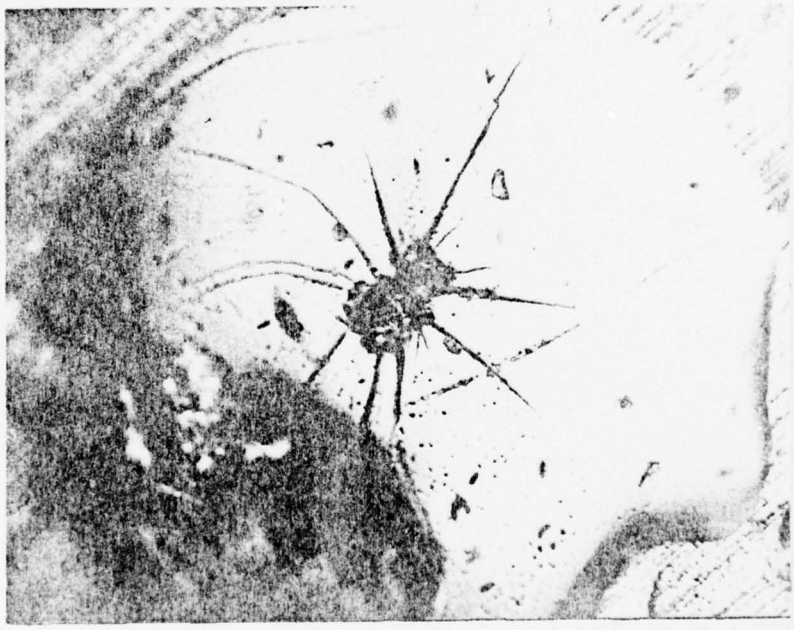

×350

Figure 31b. Crack initiation centre seen in cut away crack.

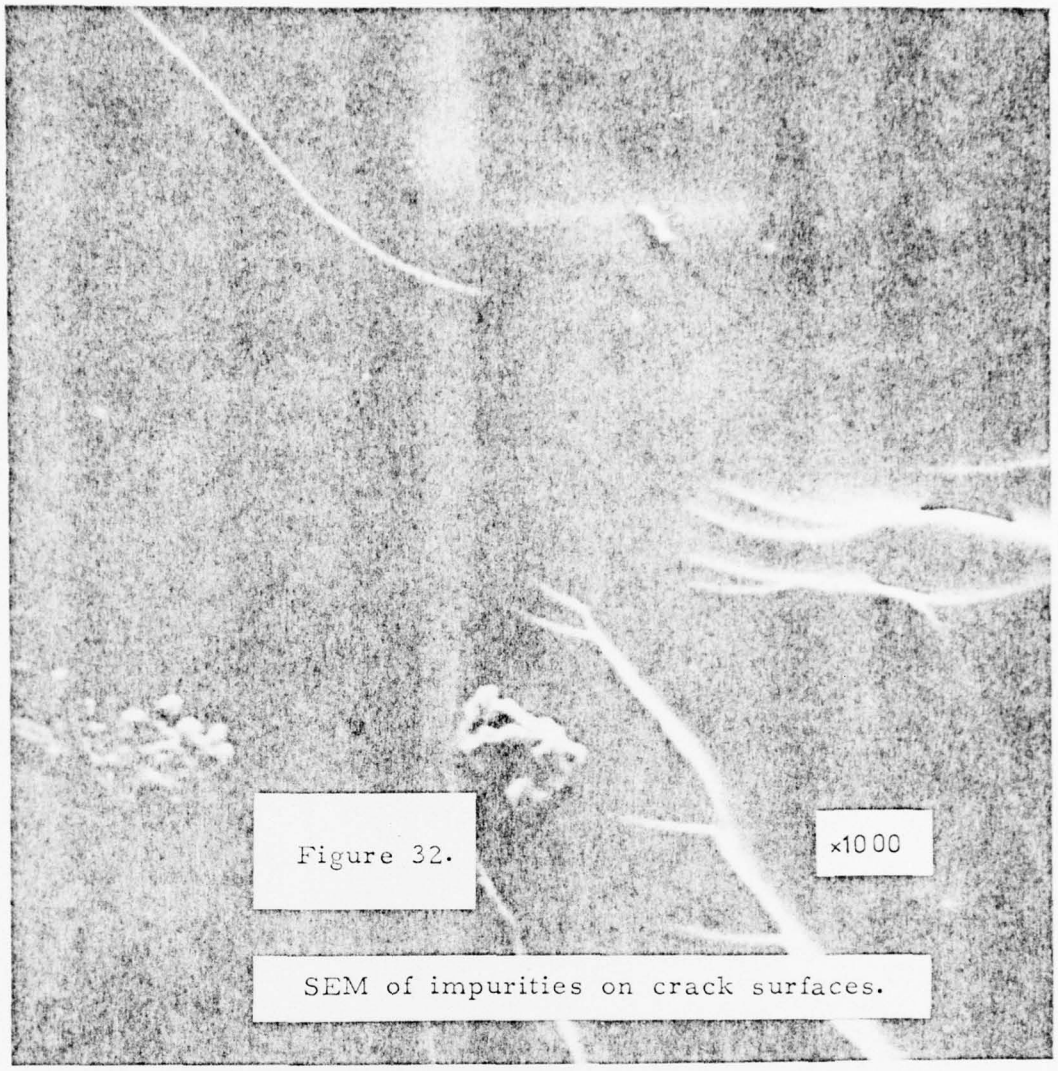

Figure 32.

SEM of impurities on crack surfaces.

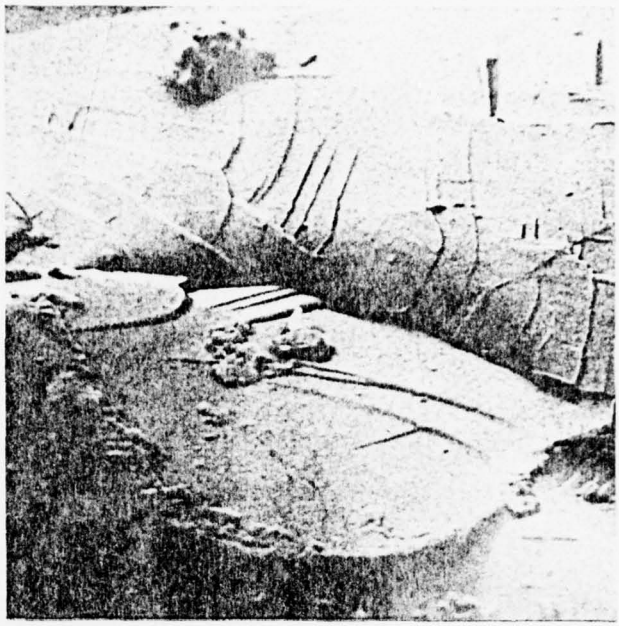

×250

×1200

Figure 33. SEM of impurities on crack surfaces.

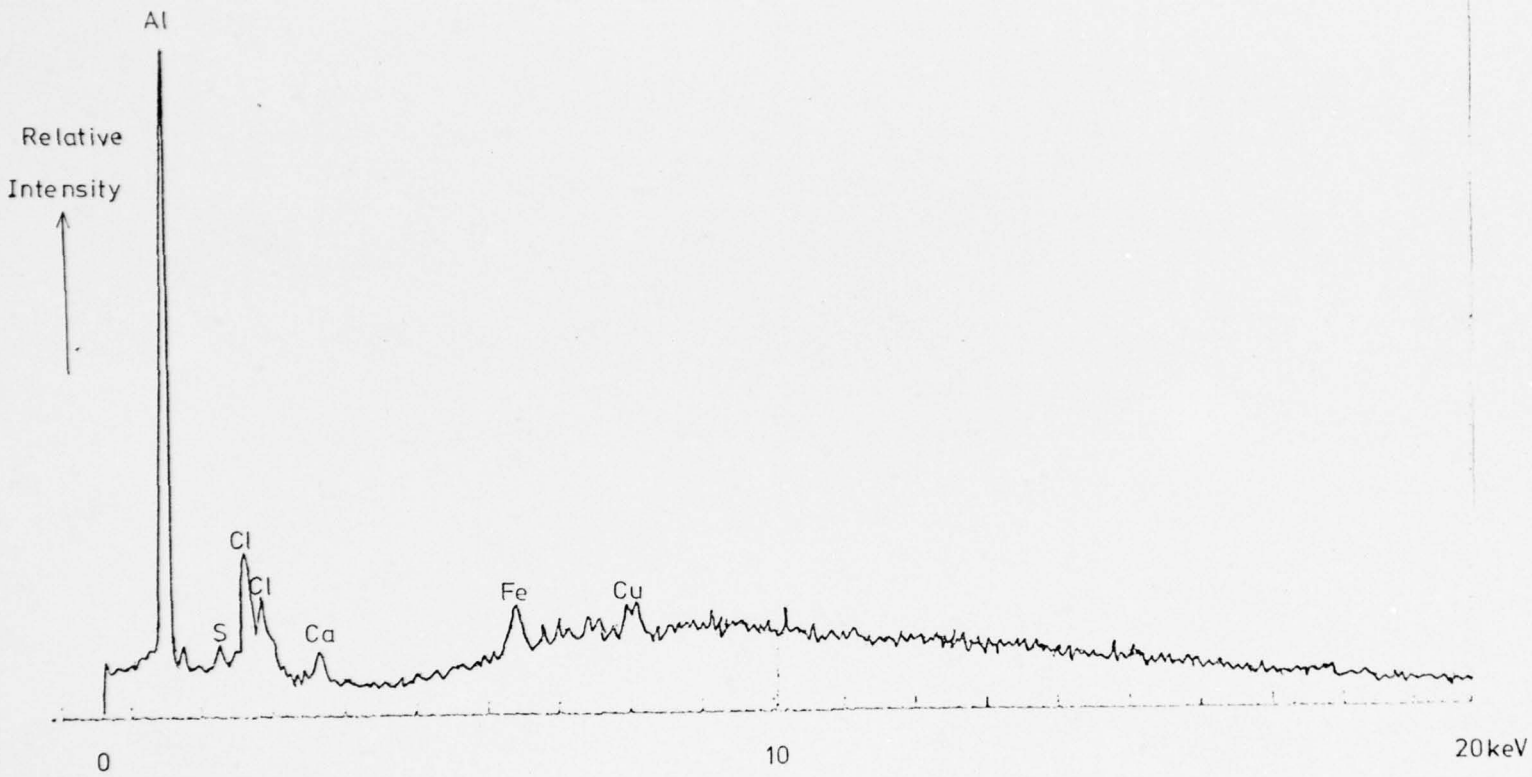

Figure 34. X-ray spectrum from particle shown in figure 32.

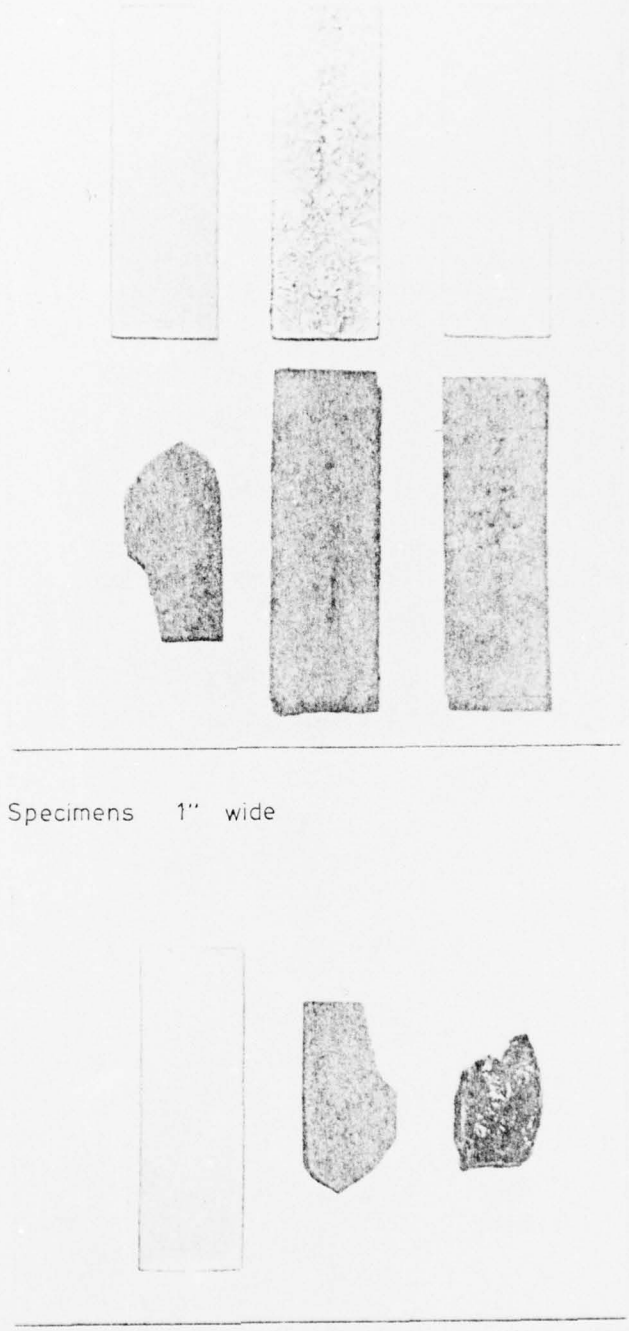

Figure 35. Stages of resin degradation

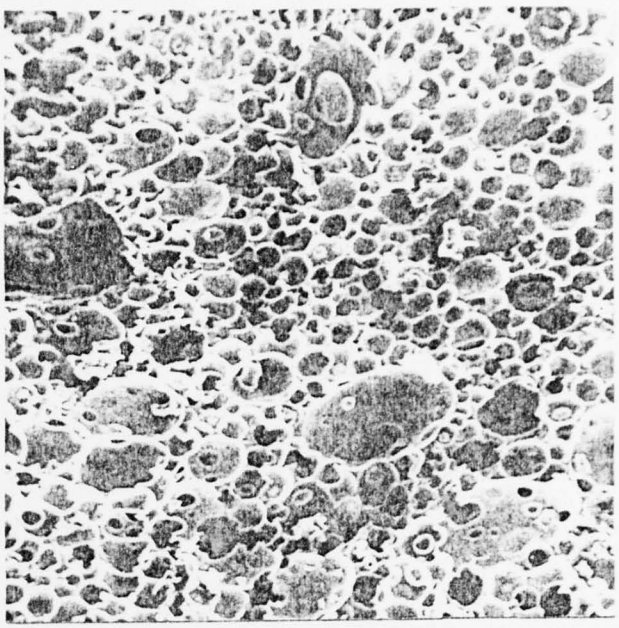

×110

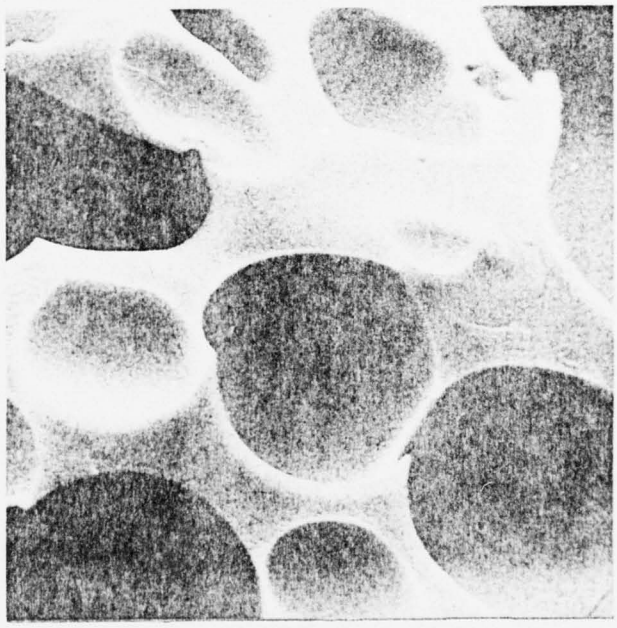

×1200

Figure 36. SEMS of internal structure after extreme degradation.

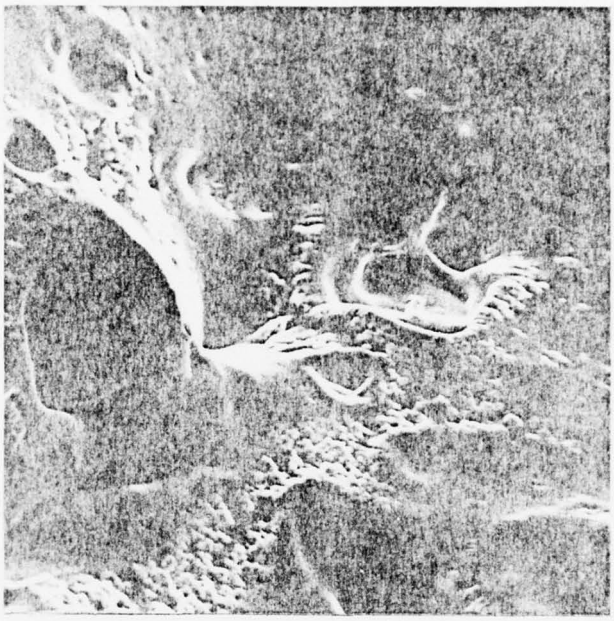

×500

Figure 37. SEMs of internal structures formed by extreme water etching.

×1000

Figure 38. SEMs of internal structures formed by extreme water etching.

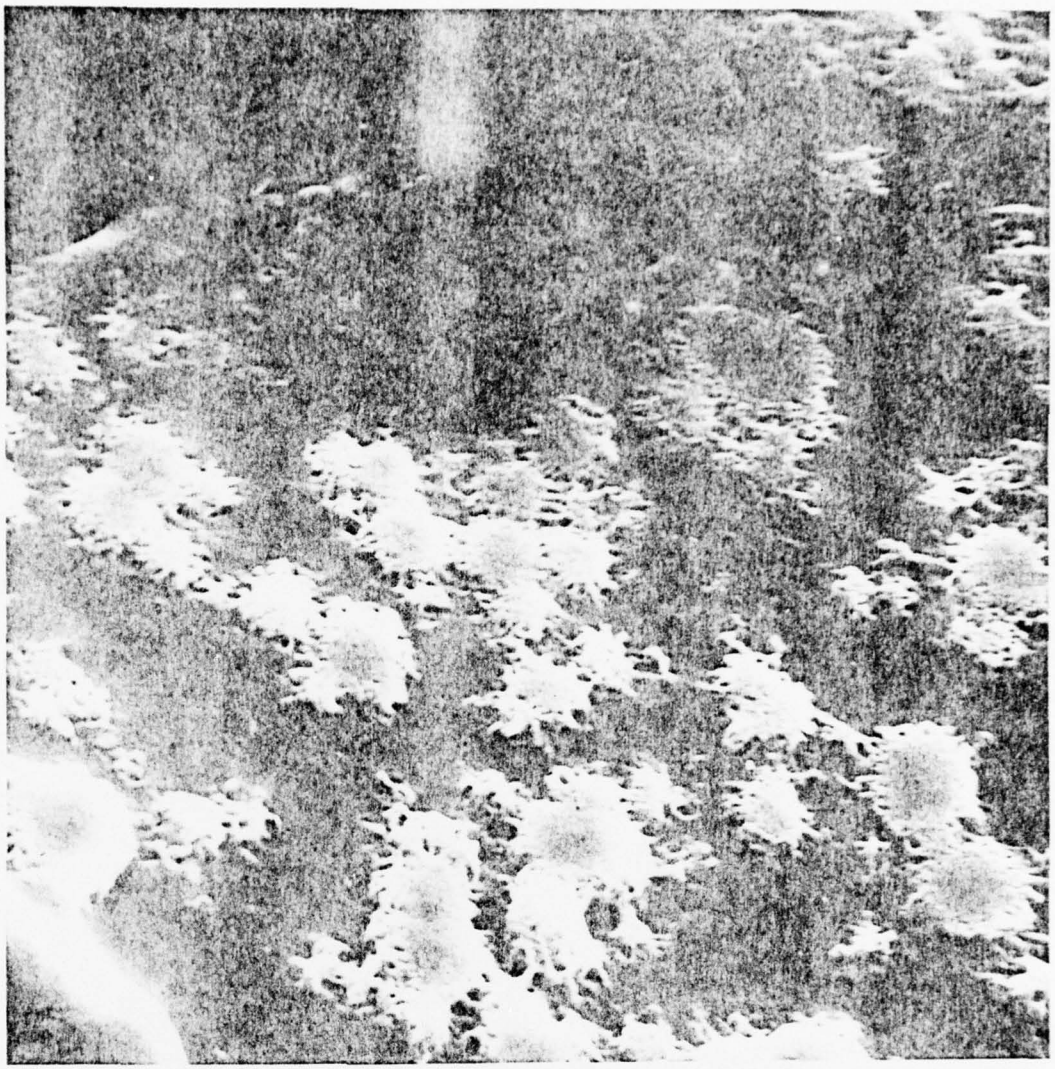

×3000

Figure 39. SEMs of internal structures formed by extreme water etching.

×250

×500

Figure 40. SEMs of earlier stages in water etching.

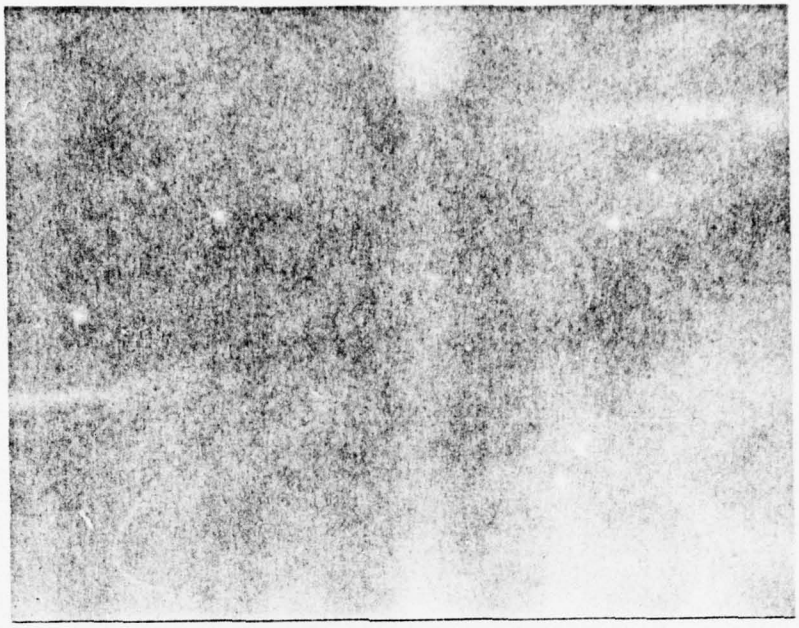

10μ fibres

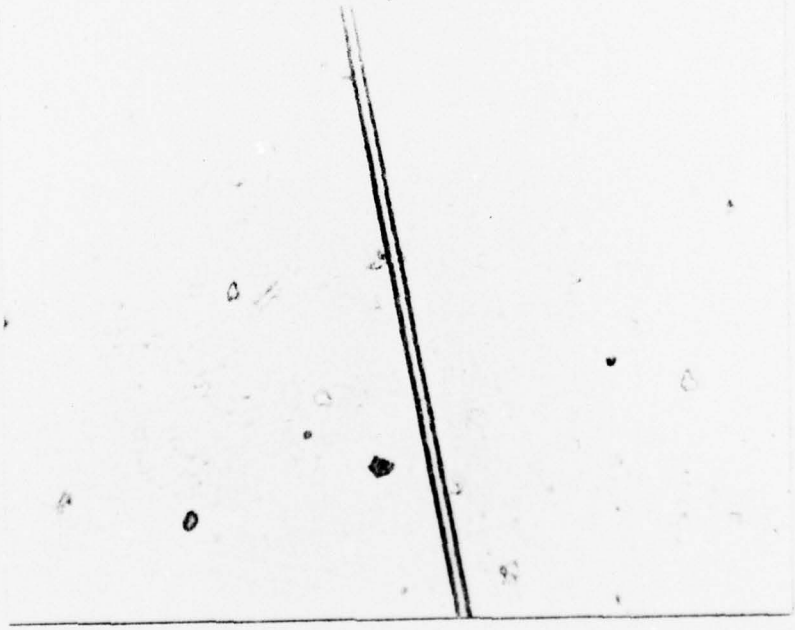

Figure 41. Glass fibres before and after debonding.

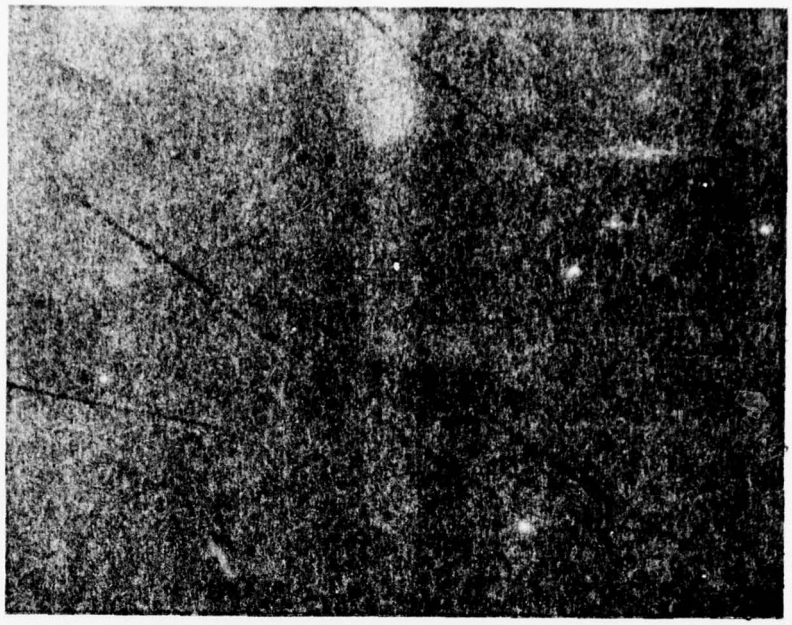

9μ fibres

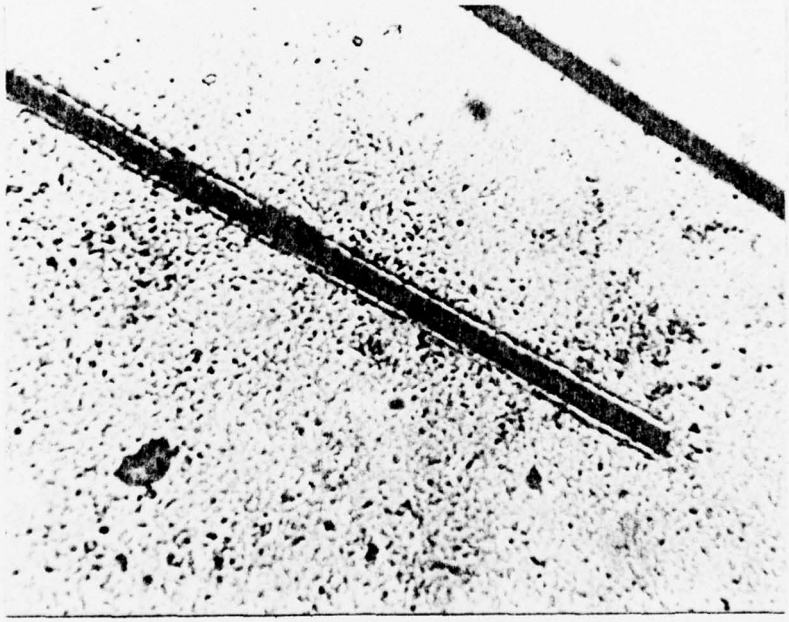

Figure 42. Carbon fibres before and after debonding.

10 μ fibre

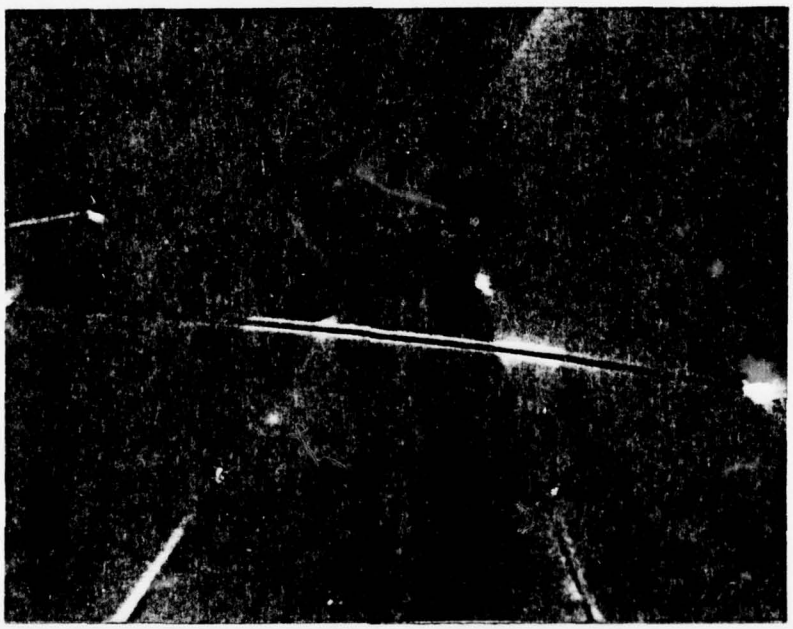

9 μ fibre

Figure 43. Stress birefringence and around glass and carbon fibres.

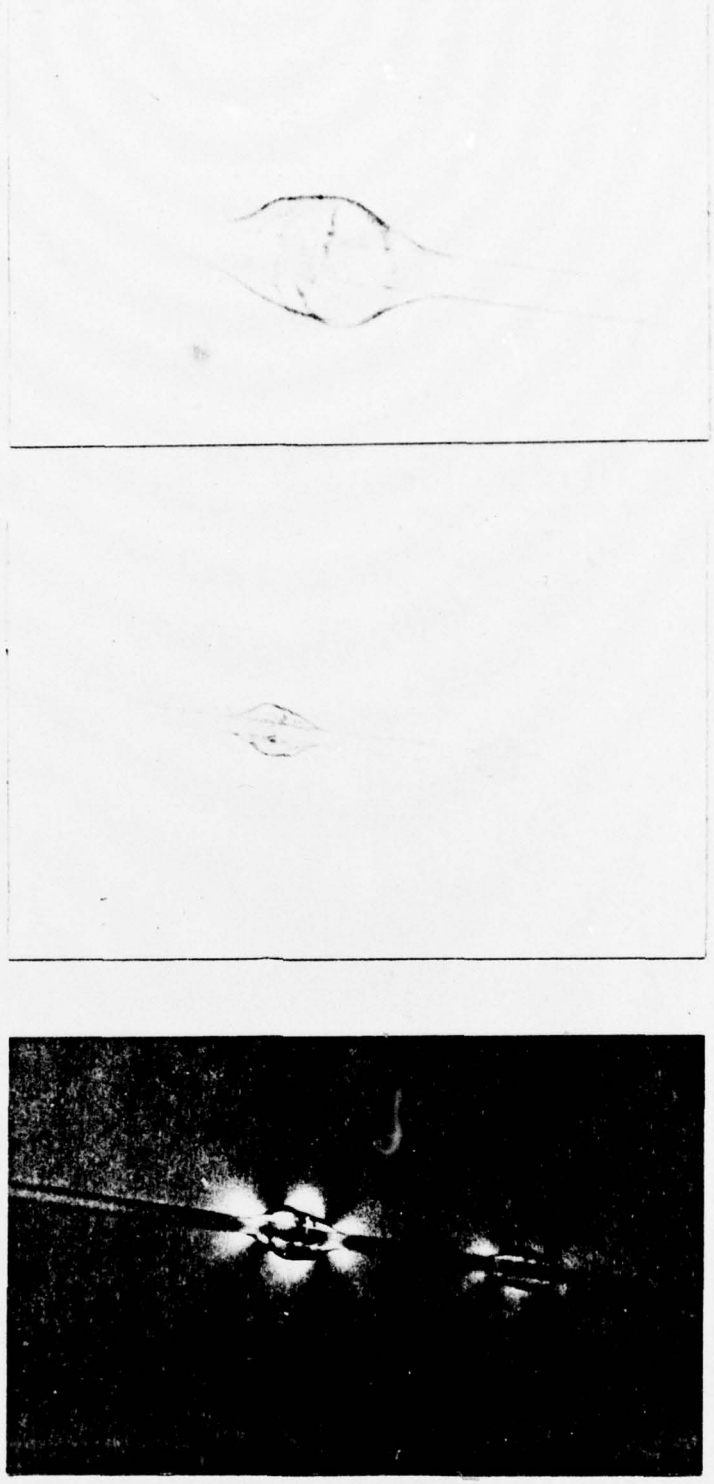

10 μ fibres

Figure 44. Surface bubbles on silane covered glass fibres.

REFERENCES

1. Ashbee, K. H. G., Frank, F. C., and Wyatt, R. C., 1967, Proc. Roy. Soc. Lond. A. 300, 415.
2. Ashbee, K. H. G., and Wyatt, R. C., 1969, Proc. Roy. Soc. Lond., A. 312, 553.
3. Wyatt, R. C., 1972, Non-Destr. Test., 5, 354.
4. Wyatt, R. C., 1975, Br. J. Non-Destr. Test., 17, 133.
5. Andrews, D. R., and Wallis, L. J., 1977, J. Phys. E., 10, 95.
6. Gutfeld, R. J. van, and Melcher, R. L., 1977, Appl. Phys. Lett., 30, 257.
7. Ratcliffe, N., and Weatherall, L. F., 1967, EMI Report DMP 2965.
8. Stone, M. H., 1968, unpublished work.
9. Lee, H., and Neville, K., 1967, Handbook of Epoxy Resins, (McGraw-Hill Inc., New York).
10. Cuthrell, R. E., 1967, J. Appl. Pol. Sci., 11, 919.
11. Schoon, T. G. F., 1970, Br. Polym. J., 2, 86
12. Kuske, A., and Robertson, G. 1974, Photoelastic Stress Analysis, (John Wiley and Sons, London).
13. Rossini, F. D., 1950, Chemical Thermodynamics, (John Wiley and Sons, New York).
14. Ashbee, K. H. G., Frank, F. C., and Du Bose, C. K. H., 1973, J. Nucl. Mater. 48, 193.
15. Frank, F. C., 1973, J. Nucl. Mater., 48, 199.
16. Frank, F. C., 1977, private communication.
17. Sack, R. A., 1946, Proc. Phys. Soc., 58, 729.
18. Sneddon, I. N., 1945, Proc. Roy. Soc. Lond. A. 187, 229.
19. Beahan, P., Bevis, M., and Hull, D., 1972, J. Mater. Sci., 8, 162.
20. Lock, M. W. B., 1972, Ph. D. Thesis, University of Surrey.
21. Wyatt, R. C., 1968, Ph. D. Thesis, University of Bristol.
22. Poritsky, H., 1934, Physics, 5, 406.
23. Wyatt, R. C., and Ashbee, K. H. G., 1969, Fibre Sci. and Tech. 2, 29.
24. Gledhill, R. A., and Kinloch, A. J., 1976, in Proceedings of the International Symposium on The Weathering of Plastics and Rubber, PRI., London.
25. Kaelble D. H., and Uy, K. C., 1970, J. Adhesion, 2, 50.
26. Kinloch, A. J., Dukes, W. A., and Gledhill, R. A., 1975, in Adhesion Science and Technology, Part B. Ed. Lee, L. H., (Plenum Press, New York) p. 597 .
27. Slater, E. A., Baborovsky, V. M., and Marsh, D. M. 1975, Proceedings of the Ultrasonics International Conference.